Chapter 01
Introduction knowledge gaps and objectives

1.1 Introduction

Al alloys have been essential materials for engineering structural applications of aerospace, aviation, automobiles, and armor applications [1–3] in the past few years due to high specific strength [4], good formability [5,6], toughness [7], corrosion resistance [8], as well as those of high electrical and thermal conductivity [9]. Some Al alloys can be heat treated to attain the desired properties, and their fabrication is also easy. Moreover, low modulus of elasticity, less high-temperature properties, and susceptivity to stress corrosion cracking (SCC) are some of their disadvantages [10]. Therefore, suitable design and development of Al-alloys are required to improve the performance of the alloys. Later, involves modification in the alloy chemistry, as well as those of control in the structures, and microstructural evolutions [1]. Such evolution may be altered through suitable heat treatments [11–13], surface modifications [14–16], and severe plastic deformation [17–21]. All the above processing techniques help us attain desired structures, and substructures [4,22–24]. Another critical factor pertains to the nature of alloying additions [25–28], combined effects of processing [29–32], and changes in alloy chemistry [33–35] is exploited in literature extensively for Al-alloys. The Al-alloys are classified into two parts: the first part relates to the wrought Al-alloys, and the second part pertains to the cast Al-alloys [4]. The Aluminium Association of America (AAA) has adopted the International Alloy Development System (IADS) for representing the Al-alloys. Accordingly, the Al-alloys are denoted by the four-digit numbers, $X_1X_2X_3X_4$. Here, X_1= main alloying element, X_2 = modification of the original Al-alloys, X3, X4 = serial number in all alloys other than 1XXX series. In the 1XXX alloy series, X3X4 shows the purity of the alloy. For instance, 1XXX series alloy offers the alloy with 99% purity. The 1200 grade alloy offers Al alloy with 99% purity, and the 1145 alloy depicts

99.45% pure Al-alloy. As per the IADS system, the wrought Al-alloys were classified into seven major types based on major alloying elements, summarized in Table 1 [4].

Table 1.1 Wrought Al-alloys designation system [4].

Serial No	Al-alloy, Serial number	Major alloying elements	Specific properties
01.	1xxx	Commercial Al with 99% purity	High corrosion resistance Excellent ductility Low mechanical strength
02.	2xxx	Copper	High strength, superior weldability, and best fracture toughness
03.	3xxx	Manganese	Excellent formability and ductility, Low strength, and corrosion resistance to construction and automobile applications
04.	4xxx	Silicon	Medium strength, Low melting point, Excellent ductility
05.	5xxx	Magnesium	Good weldability, high corrosion resistance but medium strength
06.	6xxx	Magnesium + Silicon	Good formability, Medium strength, high ductility, formability, and better corrosion resistance
07.	7xxx	Zinc	High strength, Susceptibility to SCC, and over-aging at elevated Temperature
08.	8xxx	Other elements, Ti, Ni	Medium strength
09.	9xxx	Un assigned	

1.2 Types of the Al-alloys

The two classes of Al-alloys refer to (i) heat-treatable and (ii) non-heat-treatable [4,10]. The first category of alloys (2xxx, 6xxx, and 7xxx series) could be altered on account of the heat treatments [36–39]. Moreover, the second category of Al-alloys (3xxx, 4xxx, and 5xxx

series) does not show variation in the properties if they are subjected to heat treatments [4,40,41]. The former class of alloys form metastable precipitates on account of the heat treatments [42–48]. Whereas non-heat-treatable Al alloys help control the grain size through suitable deformation [4,49]. The former class of alloys contains elements that decrease the solid solubility by reducing the temperature [10,25,35,42]. Whereas the alloys belong to the second category and do not contain such elements. Therefore, the second category of Al-alloys can be hardened if they are subjected to external deformation, for instance, hot rolling and extrusion [1,10]. The significant difference between both the alloys, on account of the alloying elements, are briefly summarised in Fig. 1.1.

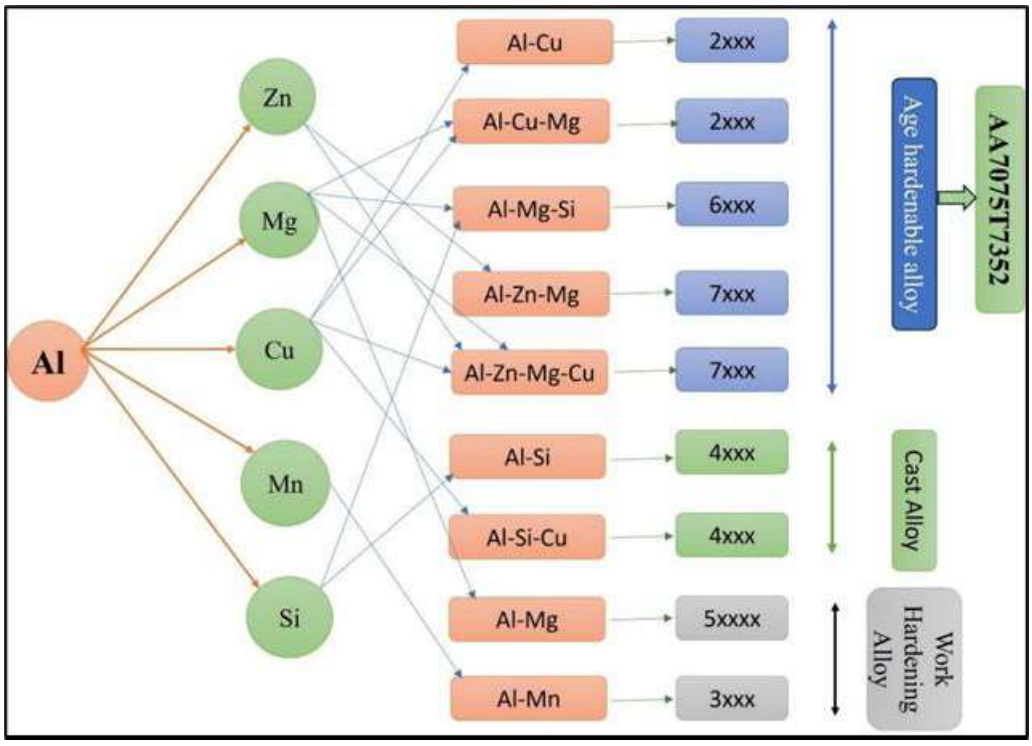

Fig. 1.1 Heat-treatable and non-heat-treatable Al-alloys.

Another representation of Al alloys is followed by specific letters on the nature of the heat treatments and the amount of external deformation [10]. Such a representation is divided into two classes. The alloys pertaining to the first class are denoted by the letter T. Whereas

the alloys related to the second class are indicated by the letter H. These letters are used as a suffix to IADS four-digit number systems. The temper designation used for the first class of Al-alloys is given in Table 1.2.

Table 1.2 Temper designations of the heat-treatable Al-alloys [10]

Serial Number	Temper designations	Applied heat treatments
01	T	Age hardened, with or without strain hardening. The second digit indicates the percentage amount of cold work
02	T1	Naturally aged at room temperature ~25 ºC after hot working
03	T2	Annealed cast alloys
04	T3	Solution treated (ST) + cold worked (CW)
05	T4	Solution treated + Naturally aged at room temperature for a long time, more than three months
06	T5	Artificially aged at 120ºC for 24 hrs
07	T6	Solution heat treated at 470 ºC, and artificially aged at 120 ºC, for the 24 hrs
08	T7	Solution heat treated at 470 ºC, and artificially aged at 120 ºC, for 24 hrs, over-aged at 160ºC for 30hrs
09	T8	Solution-treated at 470ºC for 1hr + cold worked + artificially aged at 120ºC for 24hrs.
10	T9	Solution heat treatment at 470ºC for 1 hr + artificially aged at 120ºC for 24hrs + cold worked at room temperature.
11	T10	Solution treated at 470ºC for 1 hr + artificially aged at 120ºC for 24 hrs + cold work at room temperature.
12	T85	T8 heat treatment + 5% cold rolled at room temperature
13	T7352	Solution treated at 470ºC for 1 hr, cold rolled at 10% at room temperature + artificially aged at 120ºC for 24hrs + over-aged 160ºC for the 30h.
14	RRA	Solution heat treated at 470ºC for 1 h + retrogressed at 200ºC for 20 minutes + peak-aged at 120ºC for 24h.
15	T73	Solution quenched at 470 ºC, for 1hr + peak-aged (120ºC for 24h) + over-aged at 160ºC for 30h.

In addition to the above temper designations, a few other novel heat treatments, e.g., retrogression and re-ageing, high-temperature pre-precipitate ageing, creep ageing, and creep age forming, are given to control the precipitation behaviors and mechanical properties [11,50,51], which is denoted separately as RRA, HTPPA, CA, and CAF. Moreover, the letter used to describe the work-hardenable grade of Al-alloys which is given in Table 1.3.

Table 1.3 Letters used for illustrating the work hardenable/non-heat treatable Al-alloys [4].

Serial No	Letter used for designation o the system	State of the alloy
01.	F	As fabricated
02.	H	Strain hardened
03.	O	Annealed/ re-crystallized
04.	W	Solution heat treated, the numeric value comprises the letter that signifies a distinct temperature that may vary depending on the specific system.

In the strain hardenable/ work hardenable grade of Al-alloys, the letter H1 shows hardened alloy [10]. In H1X, the second digit displays the amount of cold work, and H19 shows more than 80% asymmetric rolling. The H18 depicts fully hardened more than 75% asymmetric rolling [10]. The H16 and H14 represent three quarter hard and half hard, respectively. Moreover, H12 and H2 depict the quarter hard and work hardened+ partially annealed specimens, respectively. The H3 displays strain-hardened and stabilized alloys [10]. However, this doctoral thesis deals with the 7075 series of Al-alloy, which is heat-treatable. Hence, any aspect of Table 3 will not be discussed further.

Alfred Wilms first discovered the age hardening technique in the year 1906 by the accidental observations of variation in the hardness concerning time in the Al-Cu alloy system [52]. Age hardening refers to the controlled precipitation of the supersaturated solid solution in the nature of heat treatments. It has three major requirements. The first one relates to

decreasing solid solubility by reducing the temperature. The solid solubility of a few important elements in the α-Al matrix, concerning temperature, is briefly summarised in Table 1.4.

Table 1.4 Solid solubility of major alloying elements in α-Al [10].

Alloying elements	**Temperature of maximum solubility (ºC)**	**Maximum solubility (Wt%)**
Copper (Cu)	550	5.7
Tin (Sn)	228	0.06
Titanium (Ti)	665	1.3
Silver (Ag)	566	55.6
Manganese (Mn)	658	1.82
Nickel (Ni)	640	0.04
Silicon (Si)	577	1.65
Zirconium (Zr)	660	0.28
Lithium (Li)	600	4.2
Iron (Fe)	655	0.05
Chromium (Cr)	661	0.77
Cobalt (Co)	657	<0.02
Zinc (Zn)	443	82.8

The **second pertains** to one or more transition precipitates of the second phase, which should be coherent or semi-coherent with the matrix. Moreover, the **third requirement related to the second phase's strengthening effect should be less than that of** the alloy matrix [52,53]. The ageing process also occurs in the three stages of heat treatments. The first stage belongs to the **solutionising treatment**. In this stage, the first class of Al-alloys is subjected to 470 ºC for 1hr in the case of the 7xxx series [4], 520ºC to 570ºC in the 6xxx series [40], and 510ºC to 520 ºC for 2hrs in case of the 2xxx series of Al-alloy [54]. In this stage, vacancy concentration increases due to increased temperature [53]. The second step relates to the **water-quenching**. The alloys from the single-phase field are water-quenched. At this temperature, the alloys become supersaturated solid solutions due to decreasing solid solubility and creating vacancies. In this stage, the vacancy concentration is minimal, but

their concentration is higher than the room temperature concentration due to fast quenching. The third step is **ageing.** In this stage, the supersaturated solid solution is heated to a slightly higher temperature, 120ºC for 24hrs in the case of the 7xxx series of Al-alloy [4], 160 ºC to 200 ºC for 24hrs in the case of the 6xxx series Al alloy [40], whereas 160 ºC to 190 ºC in the 2xxx series of Al-alloy [54]. Upon ageing, the alloys form metastable precipitates depending on the chemistry of alloys in the vacancies created during the super-saturation of the solute atoms. Guinier [55] in France, and Preston [48], in England first time directly observed the experimental evidence of precipitation phenomena in the Al-Cu alloys in 1937 in the form of streaks in XRD patterns, showing the two-dimensional Cu-rich groups of atoms coherent with the {100} plane of α-Al. This was later experimentally by Nicholson and Nutting [56] by the TEM (Seimen Elmiscop I, 80kV) in 1958 in the same alloy. The unusual contrast near precipitates was seen, which was explained as Bragg's diffraction from the region distorted by elastic coherency strain. The schematic of the age-hardening technique, in the Al-Cu alloy system is shown in Fig.1.2.

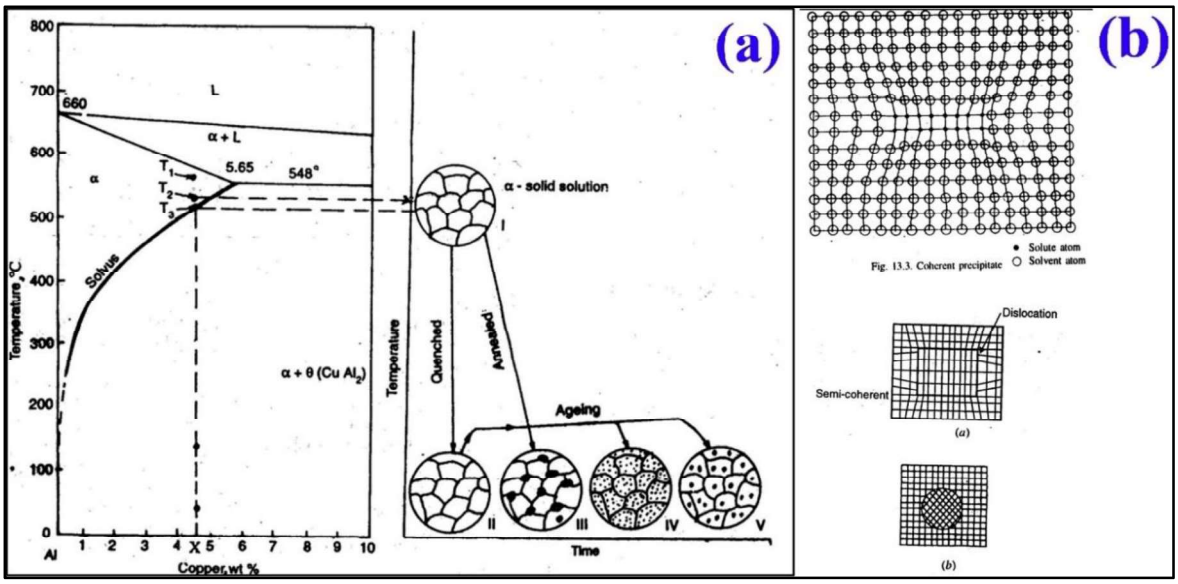

Fig. 1.2. Requirements of age-hardening: (a) decreasing solid solubility of Cu with temperature, and (b) formation of semi-coherent (θ') and in-coherent (θ) precipitates [52].

1.3 Characteristics of the Al-alloy

The major demand of the aircraft industry is to pay the high load with reduced cost as the fuel economy is directly related to weight and possesses more than 50% of the cost of the aircraft operation [1]. Wilms's discovery (1906) gave a new path to the aviation industry seeking an alloy with high strength but reduced cost [52]. After the replacement of the wood in the early 1920s,' Al-alloys become the primary airframe structural alloys. Junkers from Germany for the first time fully embraced the Al-alloy (Al-Cu) as an airframe structure in the year 1919 [1]. The current demand for modern aircraft is not only limited to the high specific strength, but they are also looking for another specific property for better designing the alloys, summarized in Table 1.5.

Table 1.5 structure property requirements of the modern aircraft design [1].

Properties	**Desirable structures**	**Function**
Strength	Fine grain size with uniform dispersion of small and hard particles	Inhibit dislocation motion
Ductility and toughness	Fine grain structures, clear grain boundary without precipitates, no shearable precipitates, and large particles	It enhances the plasticity and works hardening exponents
Creep resistance	Thermally stable particles in the matrix and grain boundaries	Inhibit the grain boundary sliding
Fatigue crack initiation resistance	Fine grain size with no shearable particles and surface defects	Prevent the stress concentration and strain localization
Fatigue crack propagation resistance	Large grain size with shearable particles, no anodic phases	Enhance the crack closure, deflection, and the slip resistivity
Stress corrosion cracking	Coarse grain boundary precipitates fine bulk precipitates, dislocation entrapment in anodic precipitates	Homogenize slip and prevention of crack propagation
High work hardening exponent	Complex dislocation structures	Restrict the dislocation motion and slip during the plastic deformation

1.4 Development of the Al-Cu (2xxx series) alloy (duralumin, Al4.5% Cu)

Duralumin, created in 1909 after Wilms discovered age hardening, was swiftly adopted by Count von Zeppelin for building rigid airships in Friedrichshafen, Germany [52]. Despite the unknown cause of age-hardening, nearly 100 airships were crafted during World War I using this alloy. Germany alone produced up to 750 tonnes of Duralumin in a single year. This aircraft featured corrugated sheeting on the fuselage for increased stiffness. Vickers in England and Alcoa in the USA also began producing Duralumin, with Alcoa introducing its version, 17S, in 1911. Over time, Duralumin's strength increased, reaching a yield strength of 280 MPa for the 2017 variant [1,52].

1.4.1 Al-Cu-Mg alloy (2xxx Al-alloy)

Advanced Al-Cu-Mg alloys, such as the wrought alloy 2024 (4.3% Cu, 1.5% Mg, and 0.6% Mn), display significant improvements in strength [1,52]. In the T3 temper, this alloy exhibited a yield strength 20% higher than Duralumin and a high tensile-to-yield strength ratio, enhancing damage tolerance. The clad version of this alloy was utilized in constructing iconic aircraft like the DC-3 and has remained the popular choice for passenger aircraft, and fuselages since then. Another noteworthy alloy, 2014 (4.4% Cu, 0.5% Mg, 0.9% Si, and 0.8% Mn), boasted a yield strength ~50% higher than Duralumin in the artificially aged (T6) state. Cold-working these alloys before artificial ageing (T8 temper) further increased their strength. Alloys based on the Al-Cu system offered superior creep strength at elevated temperatures [1]. For instance, alloy 2618 (with 2.2% Cu, 1.5% Mg, 1.1% Fe, 1% Ni, and 0.2% Si) was utilized in the skin and structural components of the Concorde aircraft. Another notable alloy, 2219 (comprising 6.3% Cu, 0.3% Mn, 0.1% V, and 0.18% Zr), was weldable and found application in fuel tanks of various space vehicles. Experimental compositions derived from this alloy, incorporating minor additions of Ag and Mg, facilitated the

formation of a stable precipitate, such as the Ω phase [1]. This precipitate, appearing as finely dispersed thin plates on the {111} α matrix planes, exhibited remarkable stability due to the segregation of these elements in the precipitate/matrix interface. Al-Cu-Mg-Ag alloys display superior creep properties to the commercial 2000 series alloys [57]. One specific alloy (containing 5.6% Cu, 0.45% Mg, 0.4% Ag, 0.3% Mn, and 0.18% Zr) exhibited zero secondary creep after being exposed to 130°C for 20,000 hours at the stress level of 200MPa in the T4 state.

1.5 Development of the Al-Li alloys

The first-generation Al-Li alloy (2020) was developed in 1958 by Alcoa to improve the specific strength of Al-Alloys [1]. Because Li is one of the most light-element among the metals, alloys belong to the light metal category with a specific density of ($0.53 g/cm^3$) [58]. Additions of each percentage of Li in the Al-alloy matrix not only reduce the weight but also enhance the modulus and specific strength by 6% and 9%, respectively [52]. German experts developed the first Al-Li alloy Scleron in the early 1930s [58]. However, the strengthening effect of Li in Al the matrix was not clear. Therefore, it was not adopted for engineering-scale production. The first-generation Al-Cu-Li alloy (2020) improves the strength and creep properties in a wide temperature range (150-200 ºC), thus making it possible for industrial-scale production [52,58]. However, these alloys contain high Fe and Si impurities and form the large insoluble Al_7Cu_2Fe, $Al_{12}(FeMn)_3Si$ intermetallic [52], which may include the crack source and cause the non-uniform strain distribution. Later, another 1420 and 1421, first-generation Al-Li alloys were developed by the Soviet Union in the year 1965 [58]. Moreover, concerns about fracture toughness, poor ductility, and processing difficulty the alloys were withdrawn from industrial-scale production, and have been gradually replaced by the 7xxx of Al-alloys [58]. To improve the problems associated with the first-generation Al-Li alloy,

the development of second-generation Al-Li alloy was started in the 1970s to 1980s to obtain high ductility, toughness, and high specific strength [1,52]. In this alloy series, Li content was increased up to 2% to increase the formation of the δ' strengthening phase, which was the primary responsible factor for improving the specific strength of alloys[58].

In the late 1980s, Polmear et al. [59] studied the impact of changes in the lithium (Li) contents (0, 0.13, 0.5, 1.0, and 2.5%) on the strength of Al-4.0Cu-0.3Mg-0.4Ag alloys. Their finding shows that maintaining the Li content within 1% gradually increased the age-hardening effect. However, when the Li content increased to 2.5%, the age-hardening impact decreased. The constituent elements copper (Cu) and lithium (Li) in the strengthening phase T1 play a crucial role in influencing the precipitation behaviors, producing a more significant strengthening effect compared to the δ' phase [60]. Nevertheless, alloys with lower Cu/Li ratios found pronounced anisotropy in mechanical properties, crack deflection, and delamination during manufacturing [10,58]. To address the issues arising from high Li content, the second-generation Al-Li alloy, Al-Cu-Li, was developed, which involves reducing the Li content while increasing the presence of the other alloying elements, for instance, magnesium (Mg), manganese (Mn), zinc (Zn), silver (Ag), and scandium (Sc)[61,62] showing an optimized developmental phase for Al-Li alloys.

The third-generation Al-Li alloys embraced complex microalloying in their composition design. Notably, the 2055 alloy developed by Alcoa in the year 2012 exhibited a tensile strength of 640 MPa in a typical T8 state [58]. Lithium and magnesium were employed to decrease density, while lithium, magnesium, copper, and silver contributed to the strengthening effect [4,10], and zinc improved the corrosion resistance [4]. Additionally, zirconium (Zr) and manganese (Mn) were included to control the recrystallization and textures [4,10]. Managing impurity elements like iron (Fe), silicon (Si), sodium (Na), and

potassium (K) plays a key role in improving fracture toughness [10]. During this period, lithium and copper content were constrained within the ranges of 1–2%, and 2–4 wt%, respectively [58]. Scholars aimed to mitigate the adverse effects of decreasing lithium content on strength by promoting the precipitations of the main strengthening phases T1 (Al_2CuLi), δ'(Al3Li), and θ(Al_2Cu) in Al-Cu-Li alloys through complex microalloying [5]. The increased specific strength on account of increasing Li content is shown in Fig. 1.3.

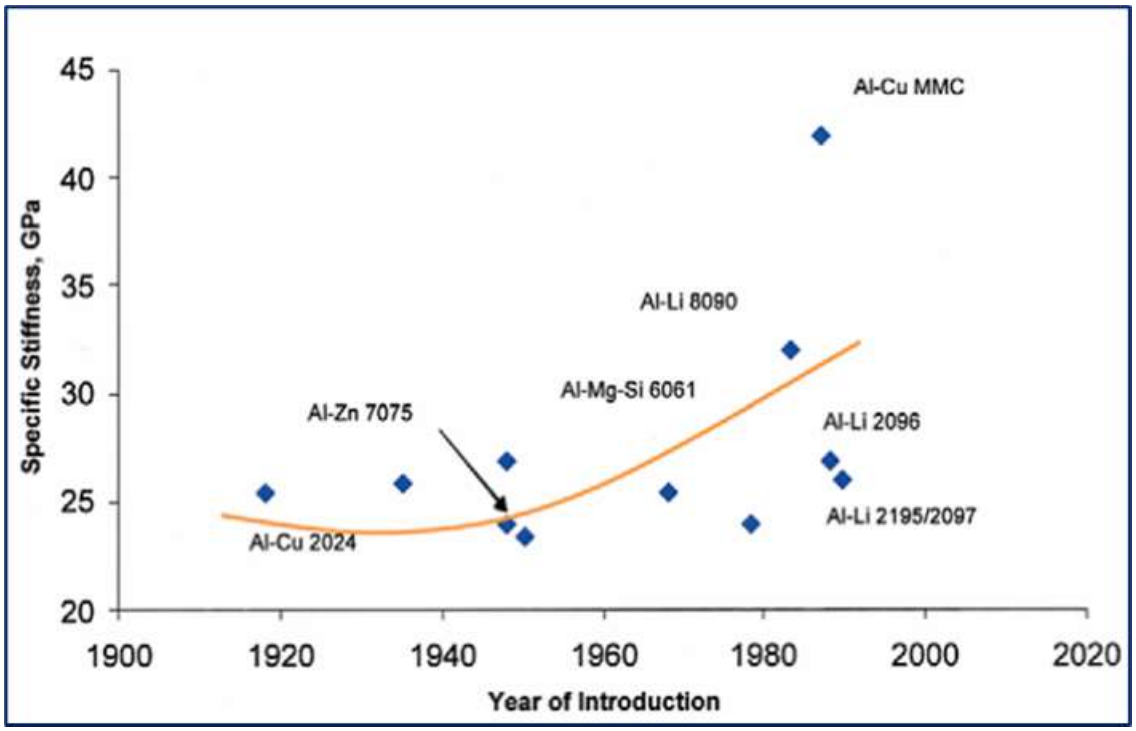

Fig. 1.3 The plots show the increased modulus of Al-Li alloys along with the year of introduction [1].

1.6 Development of Al-Mg-Si (6xxx series) alloys

While early attempts to induce age-hardening in binary Al-Mg and Al-Si alloys proved unsuccessful. Successful heat treatments were discovered for the multicomponent Al-Mg-Si alloys. The initial alloy in this category, 6051 (Al-0.5Mg-1Si), was introduced in the USA in 1921. Although not as robust as in 2017, the 6051 was more easily manufacturable and exhibited significantly higher corrosion resistance [52]. Since then, numerous wrought Al-

Mg-Si alloys have been developed, emerging as a widely used general-purpose alloy for extruded sections. The addition of the Mg and Si was carried out in the balanced proportions, leading to the formation of quasi-binary Al-Mg2Si alloys (Mg: Si, 1.73:1) or with excess Si beyond what is required to form Mg_2Si (as seen in 6051). More recently, Al-Mg-Si alloys with higher levels of Cu have been formulated, exemplified by 6013 (Al-1Mg-0.8Si-0.85Cu), boasting a yield strength of 330MPa [1,52]. Some alloys from the 6xxx series are gaining attention for automotive body sheets, mainly due to the paint-bake cycle, usually conducted at 160-190°C post-fabrication, which can additionally facilitate age hardening. Al-Mg-Si alloys with substantial Si content also find significant applications in castings. For instance, the well-known 356 alloy (Al-7Si-0.3Mg) exhibits a hypoeutectic microstructure wherein the α-Al phase is fortified by Mg_2Si precipitates, widely used for the automotive wheels and various engine components. This alloy is a notable example in this category.

1.7 Development of Al-Zn-Mg-Cu (7xxx, series) Al-alloys

In 1923, Sander and Meissner in Germany [39], recognized that certain ternary Al-Zn-Mg alloys display superior response to the age hardening as compared to other compositions explored, in that particular period. Although various countries recognized the potential of these alloys for aircraft materials, their adoption was delayed due to their high susceptibility to stress corrosion cracking (SCC) [52]. The development of an Extra Super Duralumin (ESD) reduced the weight of the zero-fighter aircraft in 1938 [40]. Upon discovery of this innovation by the Allies through the chemical analysis of a crashed aircraft during World War II, similar alloys were swiftly employed in the manufacturing of military aircraft in the USA and England. One notable example was 75S (later designated as 7075: Al-5.6Zn-2.5Mg-1.6Cu-0.23Cr), utilized for the skin and stringers of the American B-29 "Super Fortress" bomber aircraft, resulting in an immediate weight reduction of 180kg [41]. The

addition of Cu as an alloying element significantly improved SCC resistance [41], leading to the subsequent production of extrusions, forgings, and plates. The alloy 7075 gained widespread use in the post-war passenger, and military aircraft, including the popular Boeing 707 and the ill-fated Comet [52]. Over time, the demand for materials with increasingly higher strength-to-weight ratios prompted the development of the family of alloys, on account of the Al-Zn-Mg-Cu system. A recent addition to this family, AA7055 (Al-8Zn-2.05Mg-2.3Cu-0.16Zr), boasts a yield strength potentially exceeding 620MPa, with an estimated weight saving of 635 kg attributed to its use in components for the Boeing 777 aircraft [42]. The introduction of these more highly alloyed compositions has been facilitated by the concurrent development of complex multi-stage ageing tempers, some involving cold or warm working, to maintain adequate ductility, fracture toughness, and effective resistance to stress corrosion cracking.

Harold R. Kaufman, and William J. McCune, were involved in the alloy development, which was primarily composed of Al and Zn as major alloying elements [52]. To obtain the enhanced stress corrosion cracking (SCC), strength, and toughness little amounts of the Mg, Cu, and Cr are added [52]. Many researchers also found that the Al-Zn-Mg-Cu-containing alloys may produce higher strength than the alloy with a single element. Such observations led to the development of the 7075 Al alloys in the 1940s, during World War II with the introduction of AA7178 alloy [1,52]. However, less toughness makes them limited for structural engineering applications. To imbibe good toughness in them, small amounts of Fe, and Si were added and another AA7050 and AA7475 Al-alloys were developed. Al-alloys remain choice of the structural materials due to ease of the design, production, and fabrication costs. The modern aircraft A380 contains more than 60% of the traditional Al-alloys (Al-Cu) for making airframe structures [10]. For making the larger aircraft, to

transport the military equipment thicker airframe structures are required. Moreover, thick sections produced by the AA7075-T6 and AA7079T6, 7xxx series of Al-alloys are susceptible to stress corrosion cracking (SCC) and restrict their practical applications in the industry [8,10,63]. To address this issue, an over-aged 7075 Al-alloys in the T73 and T76 tempers were developed in the 1960s to enhance the SCC resistance [1,10]. Thereafter, AA7475 was developed to obtain good fracture toughness. Retrogression and re-aged 7075 Al alloys are developed in the early 1970's, to improve the strength, and SCC performances both [10]. However, due to practical difficulty, this heat treatment cannot be applied to making large parts of the airframe structures. Another, new generation of alloys AA7050-T7351, was designed in the 1970s to maintain the strength-ductility trade-off while maintaining the enhanced stress corrosion cracking performances [10]. The development of Al alloy along with their year of introduction is shown in Fig. 1.4.

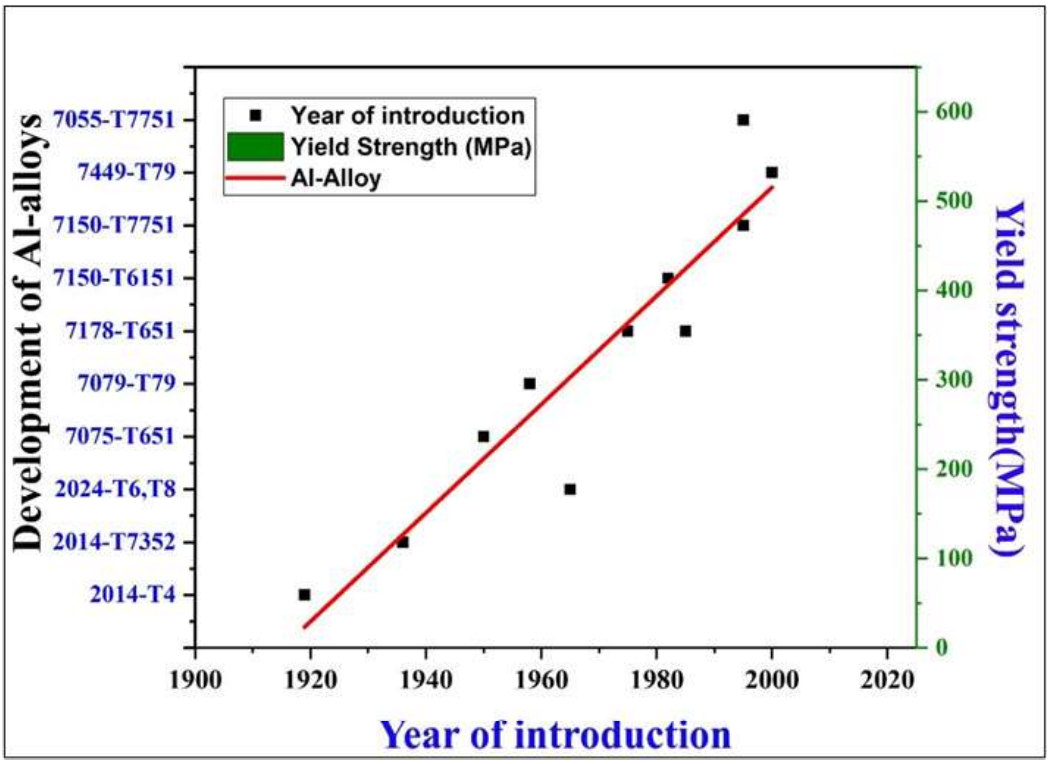

Fig. 1.4 Wings upper skin alloys and heat treatments used for manufacturing of passenger aircraft between 1919 and 1994 [1,10].

1.8 Applications of 7xxx series Al-alloys in the aerospace and armor industry

The 7xxx series (Al-Zn-Mg-Cu) of Al-alloys are extensively used in modern aircraft due to their high specific strength, for making the upper, and lower wing skins, horizontal, and vertical stabilizers, and for manufacturing the wing's stringers. For instance, AA7075-T6 alloy has been used as the main airframe structure due to its high specific strength and reduced cost. However, its susceptibility to corrosion reduced the life of airframe structures. Another high-performance alloy AA7050 was used as fuselage frames, and bulkheads in the thick plate form, and the sheet materials were used to fabricate the wing skins. The yield strength of AA7055-T7751 could reach up to 620 MPa, with improved fracture toughness and corrosion resistance. The 7075 alloys are widely used in aerospace and aviation industries for making lightweight and high-strength airframe structures [4]. The fuselage/ pressure carbin and Bullhead are made with 7075-T73511, 7075-T79511, 7105-T6511, 7175-T7951 Al-alloy [10,64], Wings, internal structures spars, ribs are made with the help of 7050-T7451 alloy [10]. The fuselage, pressure carbin, and internal structures were made with the help of 7050-T7451, 7X75-T7XXX grade of Al-alloy[1,10]. Windows and the crown frames were made using the 7175-T7351, and 7050-T7452 grade Al-alloys. Wings fuselage attachments were made by adopting the 7175-T7351, and 7050-T7452 grade Al-alloy [10, 64]. The upper wings and stringers are made with the help of 7150-T7751, 7055-T7751, 7055-T7951, and 7255-T7951 grade of the Al-alloys

The AA7017 is the Mg-Zn-based 7xxx series alloy commonly used as the armor grade Al alloys in the rolled plate form. The alloy was successfully used as armor on British and German armored ground systems. The AA7017 plate was placed in the hull portion of the UK-made warrior-tracked vehicles. Apart from the 7xxx series of Al alloys, AA 5083, AA 5456, and AA5059 were also used for ballistic resistance applications.

The conventional age hardenable Al-alloys, used for making the various parts of airframe structures are briefly summarized in Table 1.6.

Table 1.6 Applications of age hardenable Al alloys in airframe structures [10].

Product	Strength levels	Alloy/temper	Applications
Sheet	Damage tolerant	2024-T3, 2524-T3/351	Fuselage/ pressure cabin skin
Plate	Damage tolerant	2024-T351, 2324-T39, 2624-T351, 2624-T39	Lower wing covers
	Medium strength	2024-T62	Tactical aircraft fuselage panels
	Medium strength	2124-T851	Tactical aircraft bulkheads
	Medium strength	7050-T7451, 7X75-T7XXX	Internal fuselage structures
	High strength	7150-T7751, 7055-T7751, 7055-T7951, 7255-T7951	Upper wing covers
	Medium strength	7050-T7451	Spars, ribs, other internal structures
Forgings	High strength	7175-T7351, 7050-T7452	Wing/ fuselage attachments
Extrusions	Damage tolerant	2024-T3511, 2026-T3511, 2024-T4312, 6110-T6511	Lower wing stringers Fuselage/pressure cabin stringers
	Medium/high strength	7075-T73511, 7075-T79511, 7150-T6511, 7175-T79511, 7055-T77511, 7055-T79511	Fuselage stringers and frames, upper wing stringers, floor beams,seat rails

1.9 Specific properties of 7xxx series Al alloys as compared to 2xxx, and 6xxx series

The 7xxx series Al-alloys (Al-Zn-Mg-Cu) display high specific strength [65], formability [66], coefficient of thermal expansion [4], and electrical and thermal conductivity [40]. Concurrently, these also show high work hardening exponent (n), creep, and fatigue resistance [1,4]. Therefore, alloys found major applications in the aerospace and armor industries. Additionally, alloys are also used in structural engineering applications, such as making automobile components and bicycle frames [1,4]. The specific properties and their major applications are summarized in Fig. 1.5.

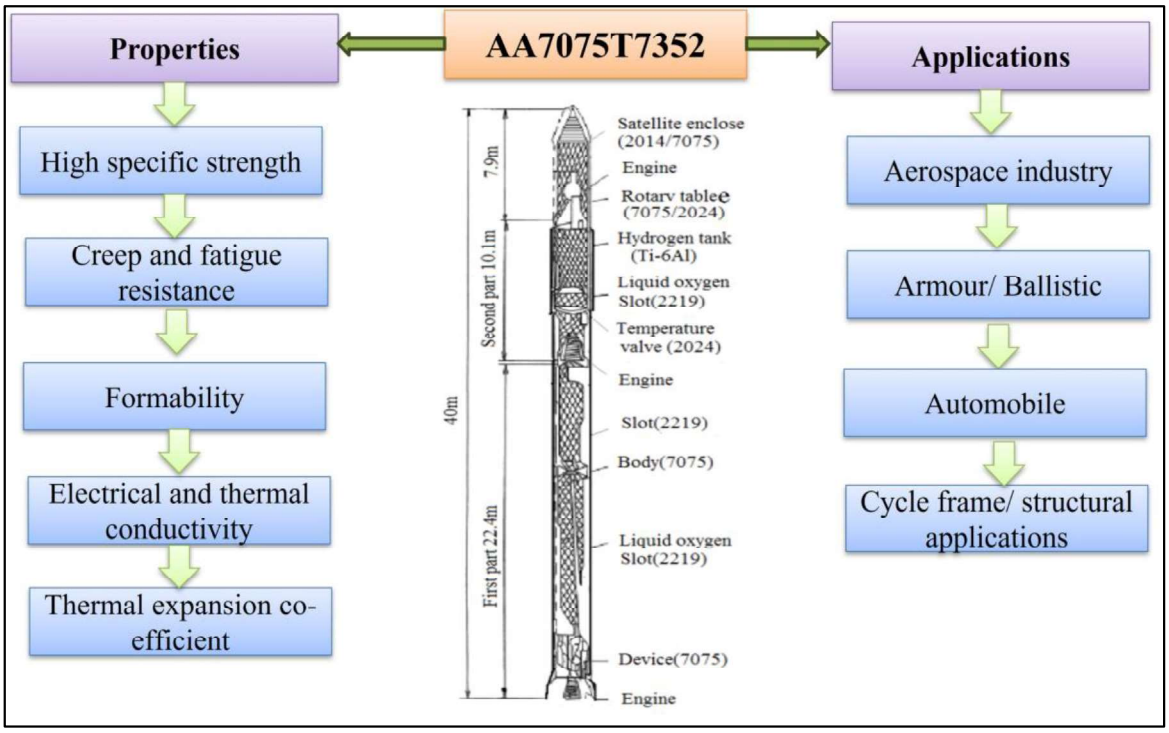

Fig. 1.5 Properties and major applications of 7xxx series Al-alloys in structural engineering applications [1].

The specific strength of the 7xxx series Al-alloy is 216 MPa.cm^3/g. On the other hand, it was reported to be 99 MPa.cm^3/g, and 58 MPa.cm^3/g for the 6xxx, and 2xxx series Al-alloys. The numerical values of specific properties of 7xxx series Al-alloy concerning 2xxx, and 6xxx series are given in Tabel 1.7. The alloy also shows more formability (~21%), as compared to the 6xxx (10%), and 2xxx (20%) alloys. In addition to this, Young's modulus (E), co-efficient of the thermal expansion, and fatigue strength were also reported high for 7xxx Al alloy which is briefly summarized in Table 1.7 [4,10,40].

Table 1.7 Comparison of specific properties of heat-treatable Al-alloys

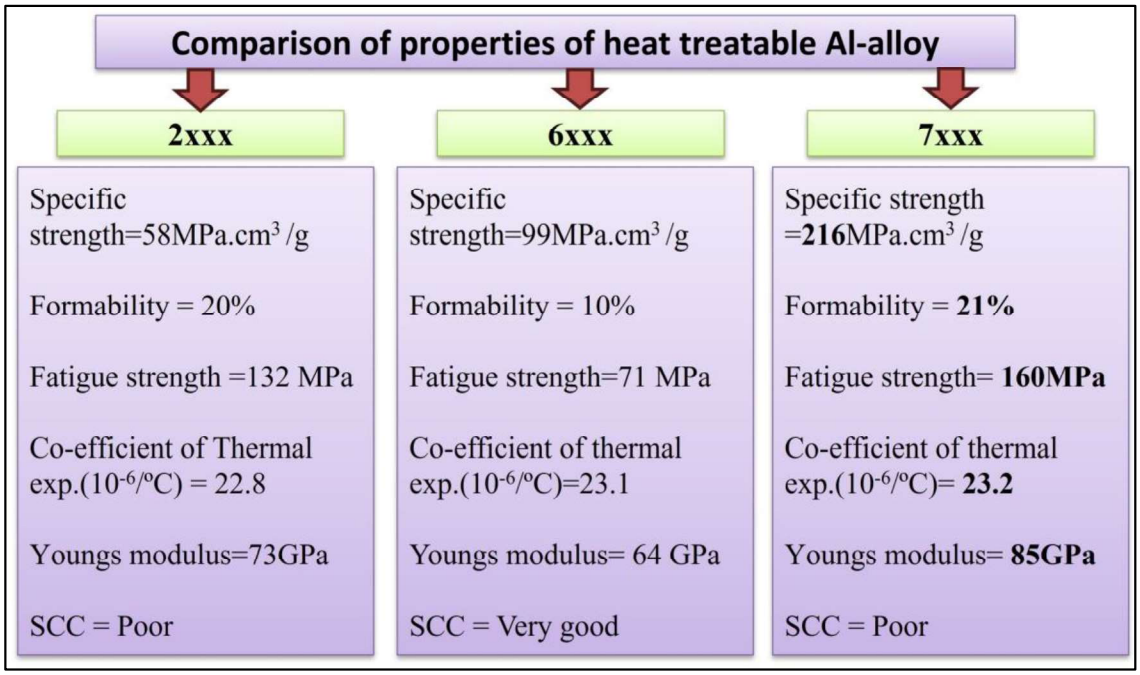

A fair knowledge of the complex phase diagrams and tight control of compositions can be used to produce a good balance between strength, fracture toughness, and fatigue crack growth resistance [1]. Therefore, phase diagrams of the heat-treatable and non-heat-treatable Al-alloys are shown in Figs. 1.6a-c, and Fig. 1.7.

1.10 Phase diagrams of the heat-treatable Al-alloys

Phase diagrams of heat-treatable Al-alloys are given in Fig. 1.6a-c. Formation of the intermetallic Al_2Cu is observed in the 2xxx series and Mg_2Si in the 6xxx series. On the other hand, the Laves phase (η, $MgZn_2$) of C14 type in the 7xxx series.

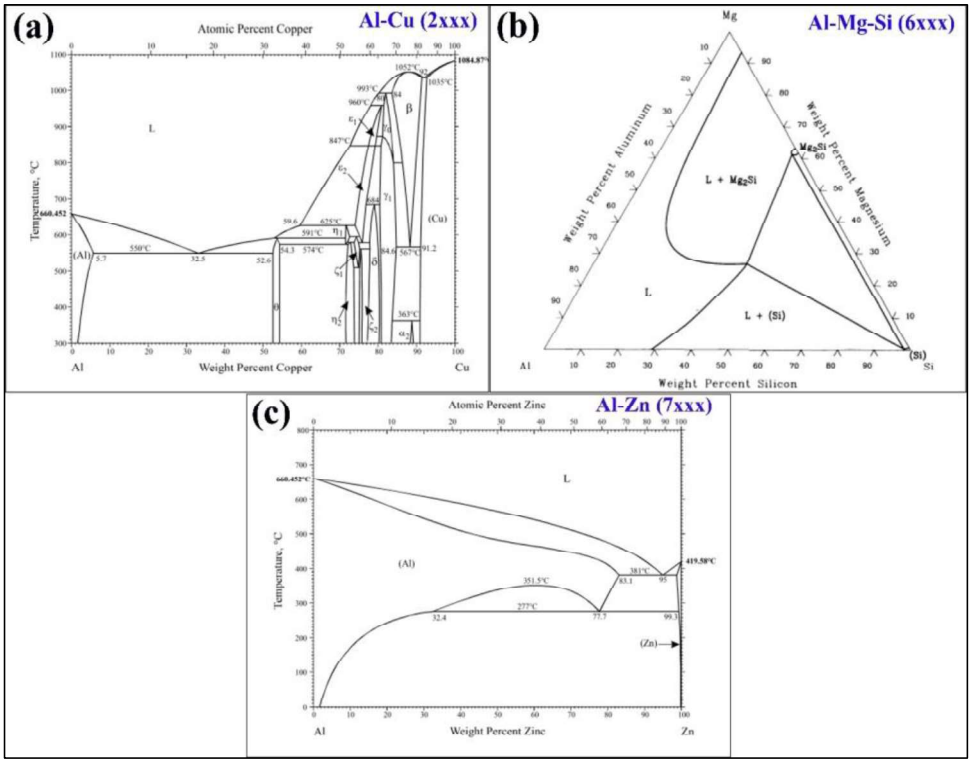

Figs. 1.6a-c. Phase diagrams of heat-treatable Al-alloys: (a) Al-Cu (2xxx series), (b) Al-Si-Mg (6xxx series), and (c) Al-Zn (7xxx) series.

In **2xxx series Al-alloys,** the precipitation sequences are summarized as Supersaturated solid solution (α)- saturated (α)- θ'' (Al_2Cu)-θ'(Al_2Cu), and θ (Al_2Cu) [4]. The GP zone and θ'' are coherent precipitates with tetragonal crystal structures, whereas θ' and θ are semi-coherent and in-coherent, respectively [67]. In the **6xxx series of Al-alloys,** precipitation sequences can be written as Supersaturated solid solution (α)-saturated (α)- β'' (Mg_2Si)-β'(Mg_2Si), and β(Mg_2Si) [40]. In these sequences, the GP zone, and β'' are coherent phases. Moreover, β' and β are semi-coherent, and in-coherent respectively [40]. **In the 7xxx series Al alloys** precipitation sequence is given as *Supersaturated solid solution (α)- saturated (α)- GP zone-η' and η ($MgZn_2$)* [47,68]. The precipitation sequences of age-hardenable Al-alloys are briefly summarized in Table 1.8.

Table 1.8 Metastable precipitation sequences in the age-hardenable Al-alloys [4].

S.N.	Alloy series	Major alloying elements	Precipitation sequences
01.	2xxx	Al, Cu, Mg	GP zone → θ'' → θ' → θ(Al_2Cu) [53]
02.	6xxx	Al, Mg, Si	GP zone → β'' → β' → β(Mg_2Si) [40]
03.	7xxx	Al, Zn, Mg	GP zone → η' → η ($MgZn_2$) for Zn/Mg ratio ≥ 2. GP-zones - η' or T' phases - η or T for Zn/Mg ratio ≤ 2 [69].
04.	8xxx	Al, Li	δ'(Al_3Li) → δ(AlLi) [58].

On the other hand, crystallographic information on various phases of heat-treatable Al alloys is briefly summarized in Table 1.9.

Table 1.9 Crystallographic information of the precipitates [112].

Al-Cu crystallographic data				
Phase	**Wt% Cu**	**Pearson symbol**	**Space group**	**Prototype**
Al	0 to 5.6	cF4	$Fm\bar{3}m$	Cu
Θ	52.6 to 54.3	tI12	I4/mcm	Al_2Cu
η_1	71.4 to 72.6	oC30	Cmmm	Al_2Cu
η_2	71.4 to 73.8	mC20	C12/m1	Al_2Cu
ζ_1	73.8 to 75	hP42	P6/mmm	Al_2Cu
ε_2	73.8 to 79.4	hP6	$P6_3/mmc$	NiAs
Cu	91 to 100	cF4	$Fm\bar{3}m$	Cu
Al-Zn crystallographic data				
Phases	Wt% Zn			
Al	0 to 83.1	cF4	$Fm\bar{3}m$	Cu
Zn	98.8 to 100	hP2	$P6_3/mmc$	Zn

1.11 Phase diagrams of the non-heat-treatable Al alloys

The 1xxx, 3xxx, and 5xxx series of Al-alloys do not follow metastable precipitation sequences, unlike the heat-treatable Al- alloys. However, the formation of some of the intermetallics e.g., $Al_{12}Mn$, Al_6Mn, Al_4Mn, $Al_{11}Mn_4$, Al_6Mn_5, were reported in Al-Mn (3xxx) alloy [1,4,40]. The Al-Mg alloy (4xxx, series) displays the formation of the Al_3Mg_2, and $Al_{12}Mg_{17}$ intermetallics. Moreover, the 5xxx series of Al-alloy (Al-Mg) shows $Al_{12}Mg_{17}$ and Al_3Mg_2, intermetallics in their phase diagram, which influences the structural and mechanical properties [40]. The work attributed in this thesis does not relate to non-heat treatable Al-alloys. Therefore, the phase diagram of Al-Mn (3xxx series) Al-alloy is only shown in Fig.1.7 due to more phase formation.

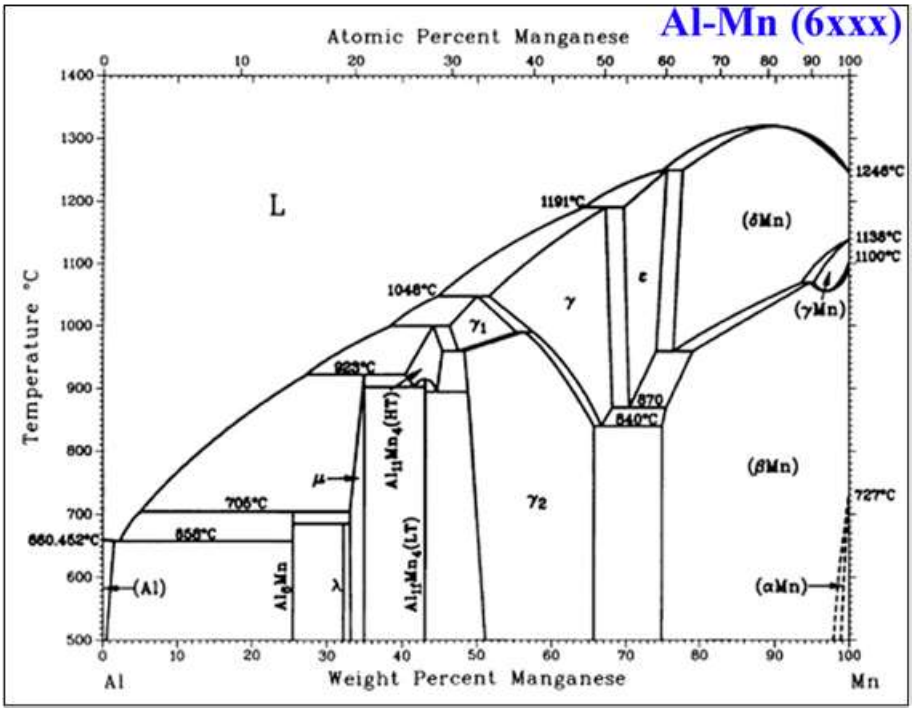

Fig. 1.7 Phase diagram of the Al-Mn (3xxx) series of non-heat-treatable Al-alloy [70].

The related crystallographic information of the 3xxx series Al alloys are given in Table 1.10.

Table 1.10 Crystallographic data of Al-Mn alloy system [70].

Phase	Composition	Pearson symbo	Space group	Prototype
Al	0.1.25	cF4	$Fm\bar{3}m$	Cu
Al_6Mn	25.2	oC28	Cmcm	Al_6Mn
$Al_{10}Mn_3$		hP28	$P6_3/mmc$	Al_6Mn
α-Mn	99 to100	cI58	$I\bar{4}3m$	α-Mn
β-Mn	75 to 100	cP20	P41,32	β-Mn
γ- Mn	95.3 to 100	cF4	$Fm\bar{3}m$	Cu
δ-Mn	76.5 to 100	cI2	$Im\bar{3}m$	W
Γ	51.8 to 68.2		$R\bar{3}m$	Al_8Cr_5
E	69.8 to 75	hP2	$P6_3/mmc$	Mg

1.12 Precipitation in age-hardenable Al-alloys

Precipitation in the age hardenable Al-alloys are diffusion-controlled solid-to-solid structural phase transformations of the continuous type [71]. These are thermally activated heterogeneous types of polymorphic transformations. The composition, and crystal structures of the parent, phase, super-saturated solid solution (α), and the product phase saturated (α) do not change as the transformation proceeds. Continuous precipitation, proceeds in all parts of the assembly. However, the rate may show significant variation in the different local regions. The original solid solution retains its identities (orientations and external shapes) throughout the reaction. Such precipitation can be represented as ‘general' and ‘localized’. In the general precipitation, the distribution of precipitates is uniform. However, in the localized precipitation, these are confined to a particular region, for example, grain boundaries of the parent phase. In this process precipitates form by the diffusion-assisted nucleation and growth process, after collecting the solute atoms by the pipe diffusion, and dislocation sweeping mechanisms.

1.13 Precipitation in the 2xxx series

Precipitation, in supersaturated Al-Cu solid solution, is extremely diverse, technologically important, and instructive in representing the nucleation mechanisms. The stable precipitate in the equilibrium state is θ(Al_2Cu), which has a tetragonal crystal structure and is fully incoherent with the α-Al.

The GP zones are fully coherent with the matrix and therefore have very low interfacial energy, therefore its precipitation starts first [72]. Whereas, the θ phase has a complex tetragonal crystal structure that can only form with high-energy incoherent interfaces, and their interfacial energy is large, therefore equilibrium θ phase forms in the last stage of the precipitation process [53].

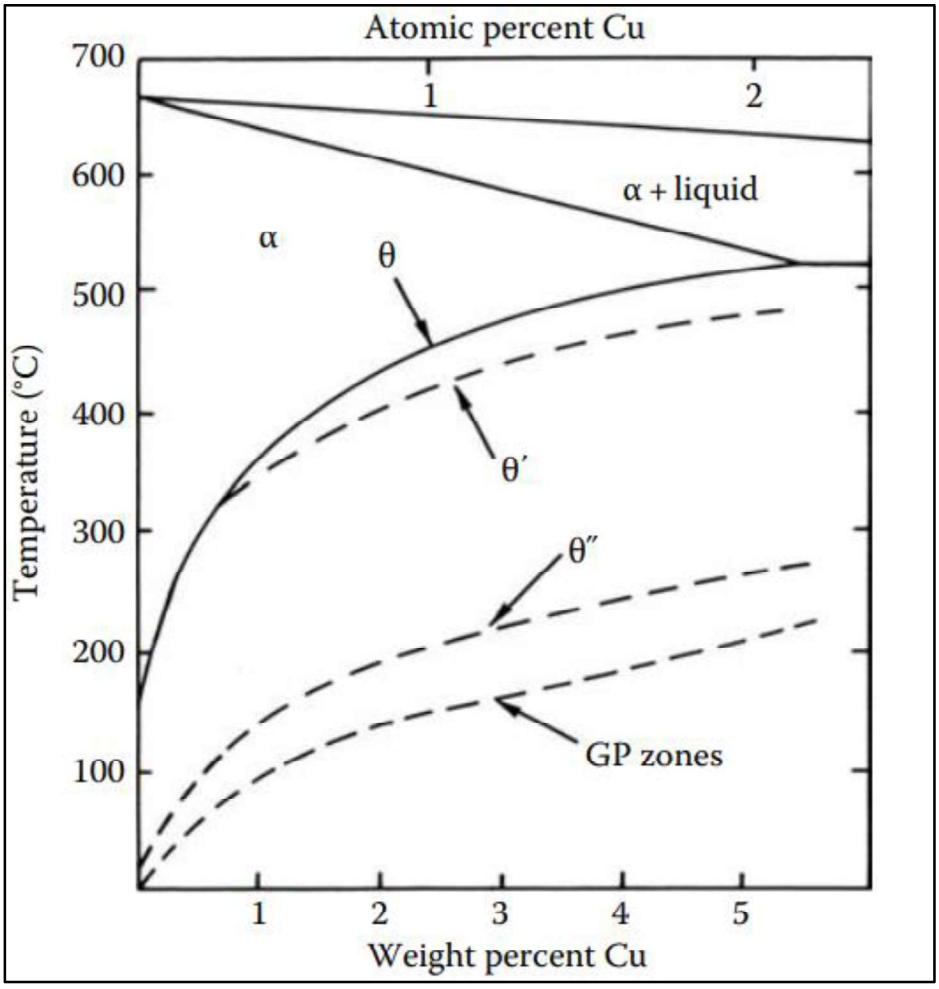

Fig. 1.8 Precipitation in age hardenable Al-Cu alloys (Duralumin Al 4.5% Cu alloy) [53].

1.14 Precipitation in 7xxx series

The 7xxx series of Al alloys are age hardenable Al alloys that follow the precipitation sequences on account of the chemistry of the alloy. For a higher Zn/ Mg ratio (≥2), the precipitation sequence could be described as Supersaturated solid solution SSSS (α) - GP-zones (coherent) - η' (semi-coherent) - η (in-coherent) [42,47,48]. Whereas, in the case of the lower Zn/ Mg ratio (≤2), the precipitation sequence is revised as SSSS (α) -GP zones - η' or T' phases - η or T [34,35,73]**.** Among all the transition (*GP zones, η'*) and equilibrium

(η) precipitates, the η' and η display orientation relationships (11 and 4 variants respectively) respective to the α-Al (cF_4, structures) [68,74], which is summarized below as:

***η'* precipitates:** η'_1 (0001) $\eta'//(1\bar{1}1)_{Al}$ $[10\bar{1}0]$ $\eta'//[1\ 1\ 0]_{Al}$, η'_2(0001) $\eta'//(1\ \bar{1}\ \bar{1})_{Al}$ $[10\bar{1}0]$ $\eta'//[1\ 1\ 0]_{Al}$, η'_3 (0001) $\eta'//$ $(1\ 1\ 1)_{Al}$ $[10\bar{1}0]$ $\eta'//[\bar{1}\ 1\ 0]_{Al}$ and η'_4(0001) $\eta'//$ $(1\ 1\ \bar{1})_{Al}$ $[10\bar{1}0]$ $\eta'//[\bar{1}\ 1\ 0]_{Al}$. ***η* precipitates:** (0001) $\eta_1//(110)_{Al}$ $[1\ 0\ \bar{1}\ 0]\eta_1//[001]_{Al}$, η_2(0001)// $(1\ \bar{1}\ \bar{1})_{Al}$ $[1\ 0\ \bar{1}\ 0]\eta_2//[110]_{Al}$, (0001)$\eta_3//(1\ \bar{1}\ \bar{1})_{Al}$ $[11\bar{2}0]\eta_3//[110]_{Al}$, (0001)$\eta_4//(110)_{Al}$ $[\bar{1}2\bar{1}0]\eta_4//[1\ \bar{1}\ \bar{1}]_{Al}$, $(\bar{1}2\bar{1}0)\eta_5//$ $(1\ \bar{1}\ \bar{1})_{Al}$ $[30\bar{3}\bar{2}]\eta_5//[110]_{Al}$, $(\bar{1}2\bar{1}0)\eta_6//(1\ \bar{1}\ \bar{1})_{Al}$ $[20\bar{2}\bar{1}]\eta_6//[1\bar{1}\bar{2}]_{Al}$, $(\bar{1}2\bar{1}0)\eta_7//(1\ \bar{1}\ \bar{1})_{Al}[10\bar{1}\bar{4}]\eta_7//[110]_{Al}$, $(\bar{1}2\bar{1}0)\eta_8//(1\bar{1}\bar{2})_{Al}$ $[0001]$ $\eta_8//[31\bar{1}]_{Al}$, (0001)$\eta_9//(110)_{Al}[\bar{1}\ \bar{1}\ 2\ 0]$ $\eta_9//[001]_{Al}$, (0001)$\eta_{10}//(1\ \bar{1}\ \bar{1})_{Al}[1\ \bar{1}\ 0\ 0]\eta_{10}//[1\bar{3}\bar{4}]_{Al}$, (0001)$\eta_{11}//(110)_{Al}[1\ 0\ \bar{1}\ 0]\eta_{11}//[1\ \bar{1}\ \bar{1}]_{Al}$.

Such precipitation forms hetero-phase and homo-phase interfaces during their evolution. For instance, GP zones, and η' form hetero-phase interfaces, coherent and semi-coherent in nature. Whereas the η ($MgZn_2$, Pearson symbol of hP_{12}) forms a hetero-phase interface incoherent in nature respective to the α-Al [11,25,75]. The η phase belongs to the Laves phases of the C14 type in the Frank Kasper Phase structure class (Space group ~ $P6_3/mm$, and Point group symmetry ~ 6/mmm) [35-37].

1.15 Factors influencing the morphology, size, and shape of precipitates

Morphologies, size, and shape of precipitates are governed by the nucleation and growth process. Precipitation in 7xxx series Al-alloys are diffusion-controlled solid-to-solid structural phase transformations, where diffusion of Mg, and Zn occurs in α-Al [71]. The energy barrier for nucleation of the metastable (GP zone, η'), and equilibrium (η) precipitates is given by Eq. 1.1 [43,58]:

$$\Delta G^* = 16\pi\sigma^3/3(\Delta g)^2 \quad \ldots\ldots(1.1)$$

Here, σ = interfacial energy of the matrix-precipitate interface. The GP zones form a coherent interface with α-Al. The shape of precipitates, in Al-Cu alloys, is summarized, on account of the mathematical relationship, proposed by Naborro [58]:

$\varepsilon = 2/3\mu_m(\Delta V/V)^2\ \Phi(c/r)$ ……(1.2)

Where, μ_m = shear modulus of α-Al, ΔV/V = fractional volume change, associated with the phase transformations, strongly influencing interfacial energy between the parent and the product phases. Here, Φ(c/r) = function of the shape of particles. The Φ(c/r) = 1, and 0.75 display evolution of the spherical, and rod-like precipitates. On the other hand, Φ(c/r) <<1, shows the formation of the product phase with a disc-shape (considering the oblate, and prolate spheroidal particles of the semi-axes r, and c) [58, 75]. The evolution of various phases, as a function of Φ(c/r) ratio is given in Fig. 1.9.

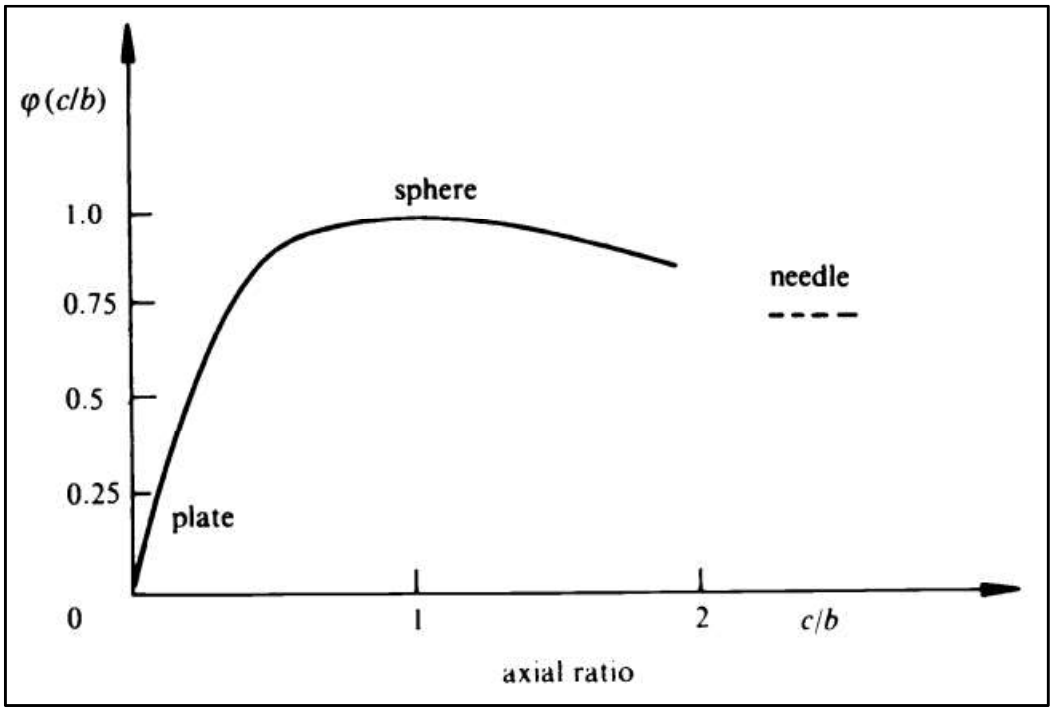

Fig. 1.9 Shape factors as a function of axial ratio for the ellipsoidal precipitates [76].

1.16 Effects of the alloying additions on microstructures and mechanical properties

Various alloying elements are often added in the heat treatable (2xxx, 6xxx, and 7xxx) Al-alloys that change the microstructures, precipitation kinetics, re-crystallization behavior, and mechanical performances specially attributed to the stress corrosion cracking (SCC). Effects of the alloying additions, microstructure evolution, and their correlation with the mechanical properties are given below:

1.16.1 Additions of the Cu+Mg

The Cu addition promotes the precipitation kinetics and formation of the GP zone in the Al-Zn-Mg-Cu alloy system. These also enhance the uniform and finer distribution of the T phase ($Mg_{32}(AlZn)_{49}$) in the peak aging state. The Cu addition also improves the thermal stability of the T phase, and the η phase was recognized as the main strengthening agent in this alloy [77]. The high-Mg, and low-Cu containing alloy forms the Al_2CuMg (S, phase) intermetallic, whereas low-Mg and high-Cu accommodating alloy forms the $Al_2Cu(\theta)$ intermetallic. The Mg and the Mg+Cu-containing alloys promote the bulk and the grain boundary precipitation. Higher Mg-containing alloys form the bulk (GP zone, η' and η), and the grain boundary (η) precipitates [78]. Therefore, additions of the Mg and Cu in the 7xxx series of Al-alloys not only form the intermetallic but also increase the volume fraction of metastable precipitates thus enhancing the yield-strength (YS), and ultimate tensile strength (UTS) by stopping the dislocation motion.

1.16.2 Additions of the zirconium (Zr)

The Zr additions in Al-Zn-Mg-Cu alloys form the Al_3Zr intermetallic, which serves as heterogeneous nucleation sites in the α-Al [79]. Thus, it promotes fine microstructure evolution and improves the mechanical properties of alloys. This also acts as a grain

boundary peening agent and reduces the grain coarsening. After Zr addition, ry-crystallization is more likely to occur, if the alloys were subjected to aging treatment and plastic deformation [27]. Hence, Zr, containing alloys results in better mechanical properties and stress corrosion cracking resistance compared to the traditional 7xxx series Al-alloys [65,80].

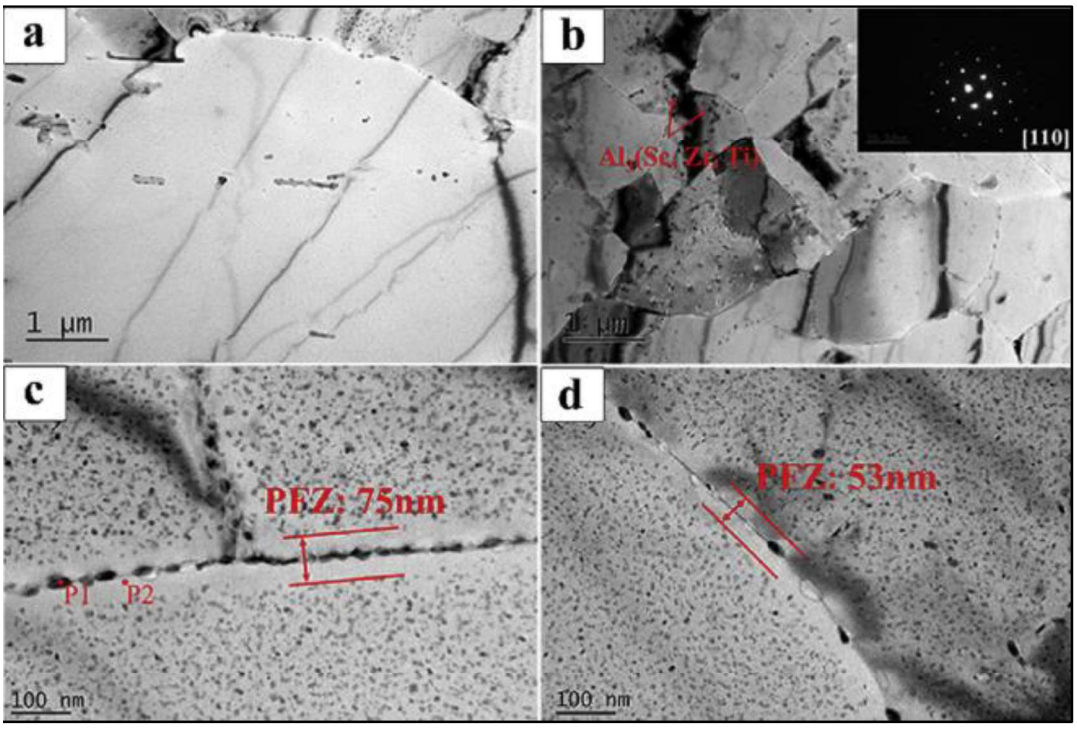

Figs. 1.10a-d. Formation of precipitate-free zones (PFZs), and intermetallic of Al_3(Zr, Ti, Sc) after alloying additions [81].

1.16.3 Additions of the Mg and Zn

Additions of Mg into Al-Zn alloys enhance the strength capabilities of this alloy system if Zn is between 3 to 8 wt% range. The combinations of the Mg and Zn, form Laves phase (η) of the C14 type $MgZn_2$, leading to a significantly enhanced response to heat treatment compared to the binary Al-Zn system. However, more additions of the Mg and Zn minimize the overall corrosion resistance of Al-alloys. Consequently, precise management of the

microstructure, heat treatment, and composition is frequently required to maintain sufficient resistance against stress corrosion cracking (SCC), and exfoliation corrosion.

1. 16.4 Additions of the Titanium (Ti)

The Ti addition in Al-Zn-Mg-Cu alloy forms Al_3Ti intermetallic, which causes thermal coarsening after heat treatment thus reducing the strengthening effect [82]. The Ti additions also improve the phase transformations from the GPII zone to the η' phase [83]. Added to this, it also acts as a matrix grain refiner during the heat-treatment [83].

1.16.5 Additions of the chromium (Cr)

The Cr is the most commonly added alloying element in the Al-Mg, Al-Mg-Si, and Al-Mg-Zn Al alloys but its amount should not exceed more than 0.35 wt%, beyond this limit Cr tends to form larger constituents with impurities like Mn and Ti. The Cr has a low diffusion rate, which forms a finely dispersed phase in wrought products inhibiting the nucleation and grain growth. If Cr containing 7xxx series Al alloys (Al-Zn-Mg-Cu) are subjected to the hot working/ heat treatment it prevents the grain growth.

1.17 Microstructure evolution after ageing of the 7xxx series Al-alloys

The ageing/ heat treatments in Al-alloys were given in different forms: (I) natural aging and artificial aging, (II) single-step and multiple-step aging, (III) iso-thermal, and non-isothermal aging, and (IV) stress-aging treatments [4]. In natural ageing, materials are aged at room temperature for more than 3 days. Artificial ageing, refers to the ageing process at slightly elevated temperature (aging at 120 ºC for 24hrs). In the stress aging treatment, a constant mechanical load is given as a part of the isothermal aging treatment. The non-isothermal aging includes two types of heat treatments heating and cooling cycle so that the precipitate

finds sufficient time for the nucleation and growth during their formation. On account of the aging treatment, and the thermal cycle, the vacancies and dislocations are annihilated [84]. In the two stages of the thermal cycle, the grain boundaries become the preferential sites for precipitation. Growth of the stabilized precipitates occurs by absorbing the solute atoms from the nearby areas of grain boundary, which minimizes the solute concentration in grain boundaries that increases precipitate-free zone (PFZs) adjacent to the boundary region [4,53].

Microstructure evolution and grain boundary precipitates are analogous to the mechanical properties, and the stress corrosion cracking (SCC) performances [85]. Uniformly distributed grain boundary "η" precipitates with wide precipitate-free zones promote failures assisted by the SCC. On the other hand, discontinuously distributed "η" with very less PFZs are desirable for obtaining enhanced mechanical properties, particularly those of strength and SCC susceptibility [36,86]. Bright-field TEM microstructures of the peak-aged (T6) alloy show continuous grain boundary precipitates and no precipitate-free zone (PFZ, Fig. 10a) [85,86]. However, fine bulk precipitates with spherical, rod, and intersecting needle-type morphologies, uniformly distributed in the α-Al matrix are another notable observation. Further, the grain boundary precipitates are coarser than the grain interior in this case [36,87]. The T76 shows fine and uniformly distributed bulk precipitates. On the other hand, coarse grain boundary η precipitates with less spacing are another observation. On T73 temper, coarse and randomly distributed spherical, plate and rod-like bulk precipitates are observed. However, grain boundary precipitates are large and their spacing is higher as compared to T6 and T76 tempers [36,87]. On retrogression, and re-aging (RRA) (Fig. 10e and f), the size of bulk precipitates and grain boundary precipitates are similar [85,87]. The spacing between

two-grain boundary (η) precipitates is larger than T6, and T76 tempers but it was close to that of T73 (Figs. 11a-f) [85,87].

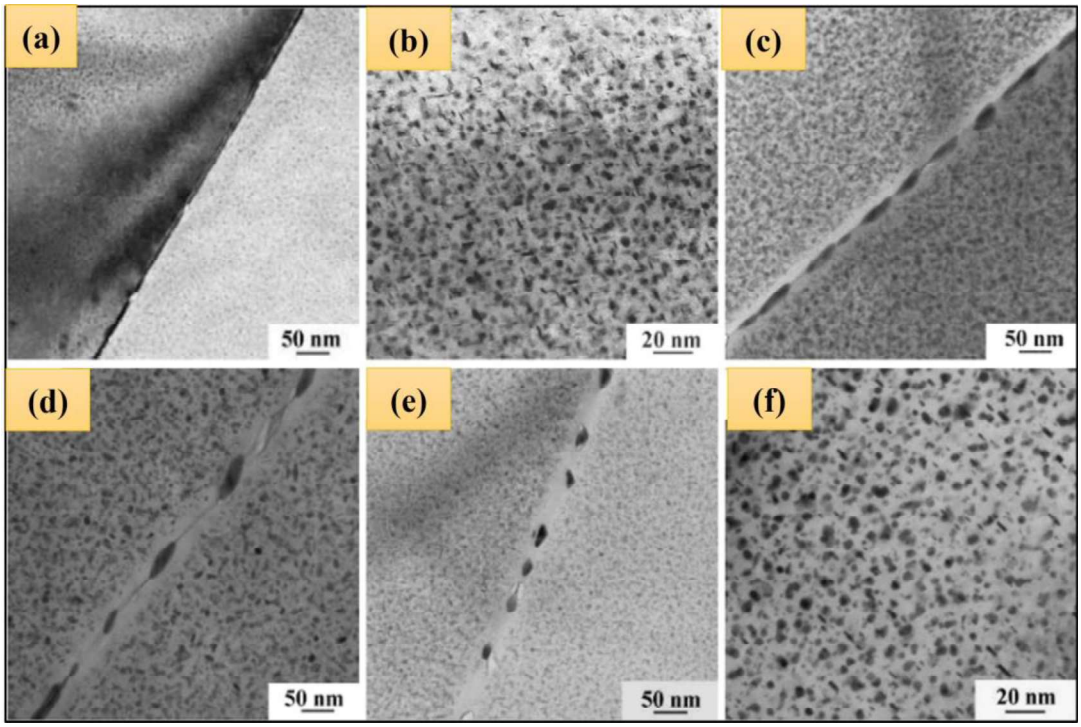

Figs. 1.11a-f. Bright-field TEM micrograph of : (a, b) peak-aged (T6, ageing at 120ºC for 24 h), (c) T76 heat treated ageing at 110 ºC for 6 hrs, over-ageing at 160 ºC for 6 hrs), (d) T73 temper ageing at 110 ºC for 6 hrs over-ageingng at 160 ºC, for 16 hrs), and (e, f) TEM microstructures of the retrogression and re-aged (RRA) 7075 Al-alloy (ageing at 120 ºC, for 24 hrs, short duration retrogression at 180 ºC for 1.5 hrs, re-ageing at 120 ºC for 24 hrs) [87].

1.18 Mechanical properties of age hardenable 7xxx series Al-alloys

Tensile strength and ductility, after plastic deformation, are functions of the size, number-density, and distribution of the ageing-induced precipitates. The engineering stress vs. engineering strain curves of the under-aged (T4), peak-aged (T6), over-aged (T73), and highly over-aged alloys were shown in Fig. 1.12 [39].

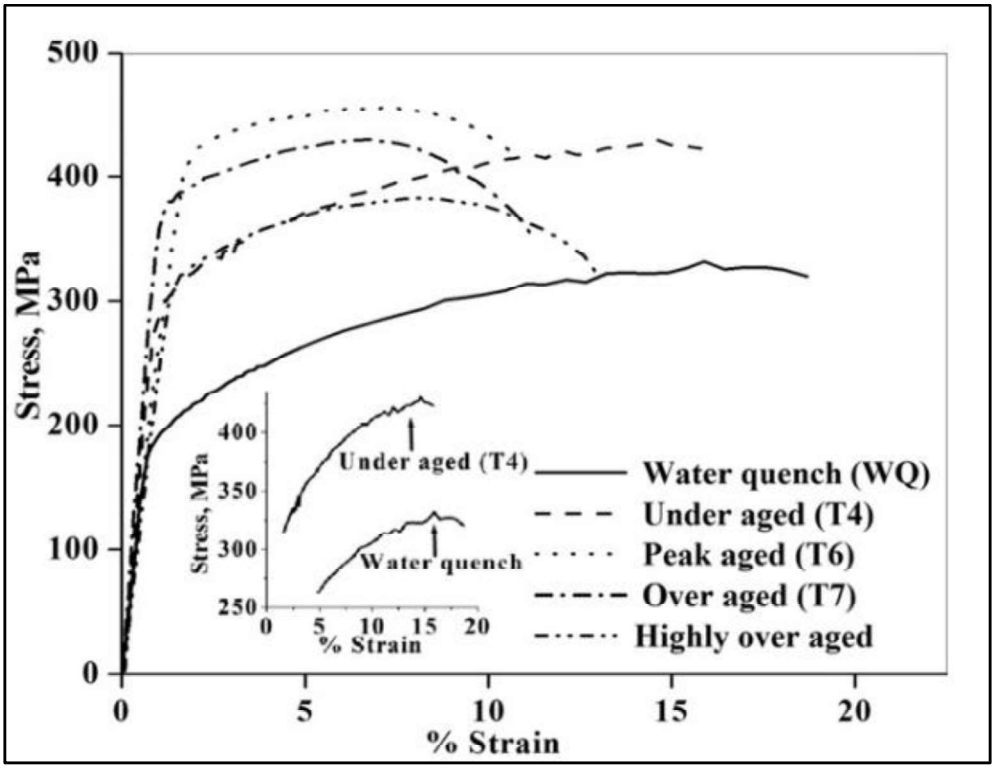

Fig. 1.12 Tensile properties of the heat-treated 7010Al-alloys, in the T4, T6, T73, and highly over-aged state [88].

The curves display maximum UTS in the peak-ageing (T6) state, whereas the water-quenched alloys show the least UTS. The ductility is least in the peak aging (T6) state, whereas the highest elongation is noticed in the water-quenching condition. Variations of the tensile properties of aged 7017 Al-alloys are reported in the works of Rout et al.[88], which is given in Table 4.

Table 1.11 Mechanical properties of the aged 7xxx series Al-alloys [88].

Tempering state	Yield strength	Ultimate tensile strength	Strain to failure (%, ε_f)
Water quenched	190	327	19
Under-aged T4	290	431	16
Peak-aged T6	400	457	11
Over-aged T73	360	431	12
Highly over-aged	313	385	13

1.19 Microstructures and stress corrosion cracking

Stress corrosion cracking (SCC) behaviors of the Al-Zn-Mg-Cu, alloy are closely related to the distribution of the η precipitates in grain boundaries [89]. Because the η precipitate is anodic respective to the α-Al. Therefore, the η precipitate serves as the active corrosion path due to the galvanic reaction between the η precipitates and the α-Al. A continuous network of the η precipitates in the grain boundary effectively enhances the SCC susceptibility. Therefore, the coarse grain boundary η precipitates and their dis-continuous network are desirable features for obtaining the enhanced SCC resistance.

The 7075 Al-alloys, in the peak-aging (T6) state, produce the continuous fine grain boundary η precipitates, which increases the stress corrosion susceptibility. Moreover, retrogression and re-aging (RRA) of the 7075-Al-alloys form a relatively coarse and discontinuous "η" grain boundary precipitate. Such precipitate formation significantly improves the SCC performances. In addition to this, Zn, Mg, Cu, Cr, and Fe are the other alloying elements added in the 7xxx series of Al-alloy, for imprving the properties [4]. Among them, Mg is anodic with the *α*-Al. Moreover, Zn, Cr, Fe, and Cu are cathodic.

Formation of the second phase particles and inter-metallics e.g. $MgZn_2$(η), Al_2CuMg, Al_7Cu_2Fe, Mg_2Si, in 7xxx series of Al –alloys [90,91], and their nature respective to the α-Al, also plays a key role for deciding the SCC performances. One notices that the standard corrosion potential value of the α-Al is -767mV. Moreover, corrosion potential values of the $MgZn_2$(η), Al_2CuMg, Al_7Cu_2Fe, and Mg_2Si precipitates are ~1095mV, -1061 mV, -654mV, and -1536mV respectively. More negative corrosion potential values of the $MgZn_2$*(η),* Al_2CuMg, and Mg_2Si make the phases anodic, respective to the α-Al. Moreover, the positive corrosion potential value of the Al_7Cu_2Fe precipitate displays cathodic behaviors with the α-Al. Hence, the presence of the *η*($MgZn_2$) precipitates in the grain boundaries of the

retrogression and the re-aged (RRA) alloy, possibly decreases the SCC performances. However, dislocation entrapment at the α-Al matrix and the η phases make them isolated and change their nature from anodic to cathodic. The multi-stage ageing is designated in such a way that it shows the formation of the GP zone, and η' precipitates in the grain interior. Moreover, coarse and discontinuous η precipitate formation in the grain boundaries, making the alloy stress corrosion cracking resistant.

1.20 Dislocation structures in cubic FCC-based metals and alloys

Strain hardening behaviors of the medium to high stacking fault energy materials are attributed to the dislocation structures evolution, during the plastic deformation [92]. Dislocation structures of such metals and alloys were well investigated in the literature on account of strain rate and the temperatures/ amount of deformation [92,93]. They found dislocation re-arrangement: as dislocation loops and forest dislocation in the first stage of the hardening curve [92]. Dislocation tangles/Taylor lattices/ Microband and cell block (CB) type of structures in the second stage [94]. Moreover, dislocation cells/ cellular wall type of structures at the beginning of the third stage [92,94,95]. It was also seen that the strain required for dislocation re-arrangement decreases while increasing the temperature. Similar dislocation structures were also noticed in the pure Al, Cu, and Ni. Moreover, second-generation MBs~ are observed in the pure Au, in addition to the above-mentioned dislocation structures [96].

1.21 Effect of friction stir processing (FSP) on microstructure evolution

Friction stir processing (FSP) is based on a similar working principle as friction stir welding (FSW) [14]. Moreover, the purpose of both is different. In the FSW the two plates or materials are joined. On the other hand, FSP refines the microstructures of the same plate being processed [23]. In the nugget zone, fine grains are formed due to severe plastic

deformation, and thermal effect [97]. As a result, FSP has been employed for a wide range of applications. These include achieving ultra-fine-grain structures, maintaining the compositional and microstructural homogeneity, producing the hybrid and in-situ surface, bulk metal matrix composites in materials like Al-alloys, high entropy alloys, Mg-alloys, Cu-alloys, and other high-strength materials [22]. Additionally, FSP has been utilized for repairing cracked or defective components, improving resistance to HAZ liquation cracking, enabling additive manufacturing, enhancing super-plasticity, and various other purposes [98,99]. On account of differences in thermal environment and plastic deformation, various microstructures evolved in the processed zones across the transverse direction. The onion ring, CDRX, equiaxed, and fine grains are observed in the nugget zone [100,101]. The onion ring appears due to successive shearing of the semi-cylindrical plastic material layers from the front of the tool, and their deposition from the side [22,101]. The grain structure evolution in SZ is complex and mainly driven by the CDRX and the GDRX. On the other hand, particle-simulated nucleation (PSN) plays a minor role [102,103]. The CDRX occurs when strain and the strain rate are high [104].

The CDRX is characterized by a refined and the equiaxed fine grains concurrently with the higher fractions of the high-angle grain boundaries [22]. The refined and the equiaxed grains are due to strain-induced progressive rotations of sub-grains by absorption of the dislocations in the grain boundaries followed by the increased misorientation and their gradual transformations in the grain boundaries [105]. In the GDRX flattened and serrated grains were formed due to dynamic recovery induced by the deformation, which intimate, and annihilate to form the equiaxed grains [22,103]. DDRX is not common in Al-alloys due to high recovery [103]. The microstructures in the TMAZ are due to dynamic recovery because of the temperature, and strain-induced, while plastic deformation in this region is not

sufficient for the re-crystallization [14,106]. The grains in this narrow zone are elongated and relatively coarser than the nugget-zone, after FSP [107]. The grains in the HAZ are coarser due to the thermal effect without plastic deformation [103]. Due to the shoulder-affected zone (SAZ), and the pin-affected zone (PAZ) in the nugget region, there are through-thickness variations of the microstructures down the weld nugget [22,107,108]. The pin diameter also varies from the top to the bottom regions of the processed zone. Such variation changes the temperature distribution, and effective strain in the nugget zone [14,109]. A Schematic of the FSP set-up is given in Fig. 1.13, and the resultant microstructure evolution along various zones of the processed region is given in Figs. 1.14a-e.

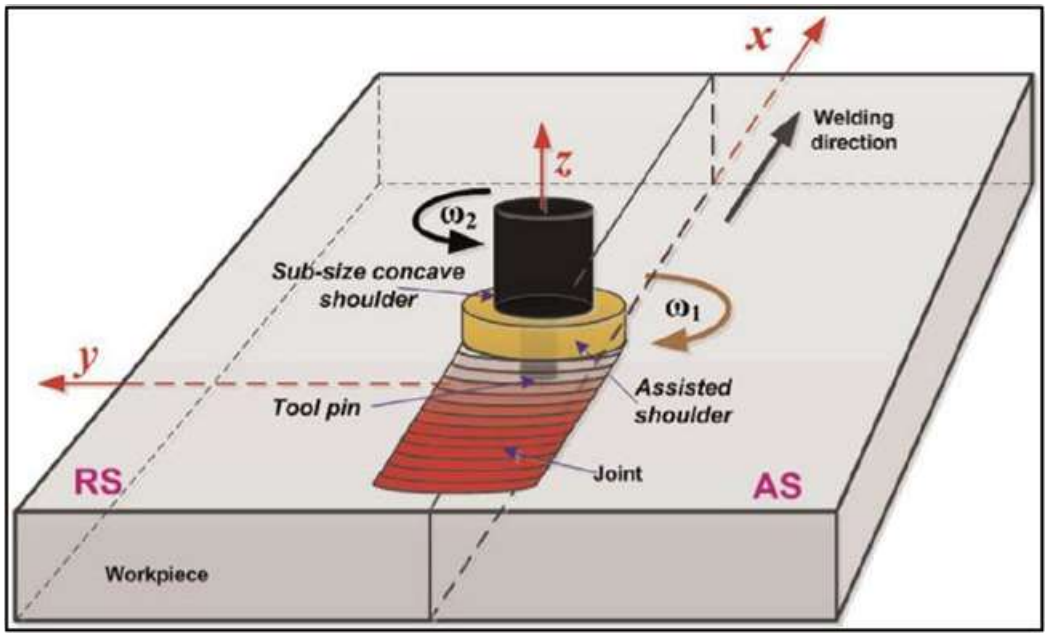

Fig. 1.13 Schematic of friction stir processing containing the tool and the workpiece, as well as the processed region [22]

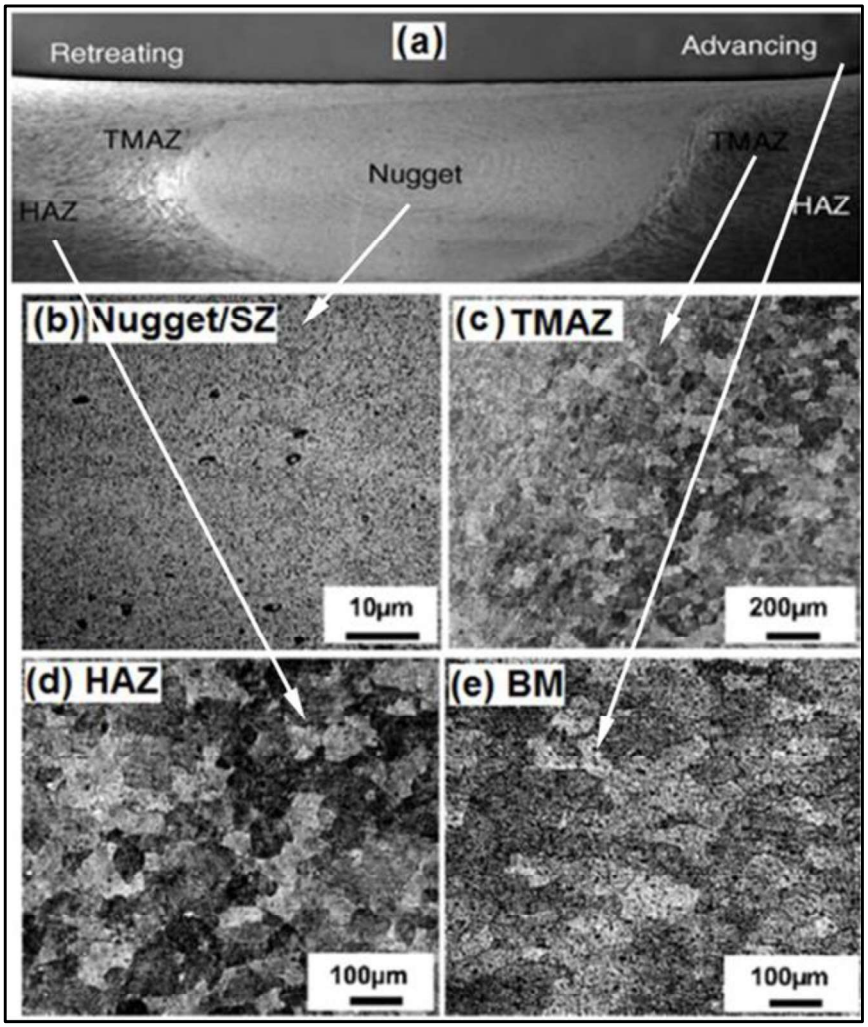

Figs. 1.14a-e. Microstructures variation throughout the processed zone: (a) macrostructures, (b) nugget zone, (c) thermo-mechanically affected zone (TMAZ), heat affected zones (HAZ), and the base-metals (BM) [22].

1. 22 Textures in cubic FCC-based metals and alloys

The sum of the crystallographic orientation of crystallites within a polycrystalline aggregate of materials is known as the texture [110]. This could be represented in two ways, the first way relates to the pole figures method, and the second pertains to the orientation distribution function (ODF) method [111]. The former gives qualitative information of orientation representation, which could be denoted as {111}, {200}, {220}, and {311} pole figures[110]. Whereas, the latter can be used to describe the texture quantitatively in terms

of the texture components, which comprise a crystallographic plane, and the crystallographic directions [111]. The crystallographic plane lies in the normal direction, whereas the crystallographic direction is parallel to the rolling direction. The ODF plots of FCC materials are illustrated by the constant Φ_2 sections with iso-intensity contour in the Euler space denoted by the three Euler angles (Φ_1, Φ, Φ_2) as per the Bunge notations, which are three consecutive rotations given to the specimen reference frame (RD, TD, and ND) to coincide with the crystal reference frame (100, 010, and 001) [39,40].

The stacking fault energy (SFE) mainly influences the texture characteristics in the FCC-based cubic metals and alloys, which are divided into two groups. The first group relates to the pure metals type texture with high stacking fault energy (High SFE), and the second pertains to the alloy type texture with low stacking fault energy (Low SFE) [111]. Slip is the deformation mode for those materials having high stacking fault energy (High SFE) which is around 170, 130, and 70mJm^{-2}, and known to form the pure metal type texture. The pure Al, Cu, and Ni belong to such type of materials [113]. The materials with low stacking fault energy (SFE< 25mJm^{-2}) display the alloy-type texture. The austenitic stainless steel, 70-30 brass, Ag, and the solid solution strengthened Ni-based alloys typically show such textures [113].

Texture can also be classified on the account of the deformation, and heat treatments. Re-crystallization texture was developed, if the alloys were subjected to heat treatments. Moreover, if alloys were deformation, the deformation textures were developed. Combinations of heat treatment and deformation result in the deformation and re-crystallization of textures [111-112]. Such textures (re-crystallization+deformation) were often observed in the hot rolled, and the friction stir processed metals and alloys.

The as-cast materials display re-crystallization and solidification textures, and coarse grain structures due to the growth of dendrites in a particular direction [111]. The preferred alignment of the columnar grains in heat flow direction influences the overall solidification/ cast texture of the materials. Such solidification texture gets modified in the various stages of the thermo-mechanical processing. The texture of the hot rolled materials comprises both the deformation and re-crystallization textures, whereas hot rolled +annealed, and cold rolled+ annealed alloys display the recrystallization textures. On the other hand, cold-rolled alloys display deformation textures, rolling followed by annealing shows both textures. The FCC recrystallization, textures are given in Table 1.12 [114–116].

Table 1.12 Typical FCC re-crystallization textures [62,63].

FCC recrystallization textures			
Components	**{hkl}<uvw>**	Euler angles (Φ_1, Φ, Φ_2)	Symbols
Cube	{001} <100>	0°,0°,0°/90°	Cu
Cube RD	{013} <100>	0°, 22°, 0°/90°	Cu R
Cube ND	{011} <310>	22°,0°,0°/90°	Cu N
Cube-twin	{122} <212>	27°, 48°, 27° or 63° 48°, 63°	Cu T
Goss	{011} <100>	0°, 45°, 0°/90°	G
B_R	{236} <385>	80°, 31°, 35°	B_R
U(transition)	{258} <121>	45°, 35°, 20°	U
R	{124} <211>	53°, 36°, 60°	R
P	{011} <122>	65°, 45°, 0°/90°	P
Q	{013} <231>	45°, 15°, 10°	Q

The deformation textures observed after cold rolling and cold rolling followed by annealing are given in Table 1.13.

Table 1.13 Typical FCC deformation textures in metals and alloys [115].

Texture components	**{hkl}<uvw>**	**Euler angles (Φ_1, Φ, Φ_2)**	**Symbols**
Copper	{112} <111>	90°, 30°, 45°	C
S	{123} <634>	90°, 30°, 45°	S
Brass, Bs	{011} <211>	59°, 34°, 65°	Bs
Goss, G	{011} <100>	0°, 45°, 0°/90°	G

The extensive information on textures as the function of the spread of orientations could be described within a three-dimensional Euler's space. The FCC-based metals/ alloys display four fiber textures illustrated in Fig. 1.15.

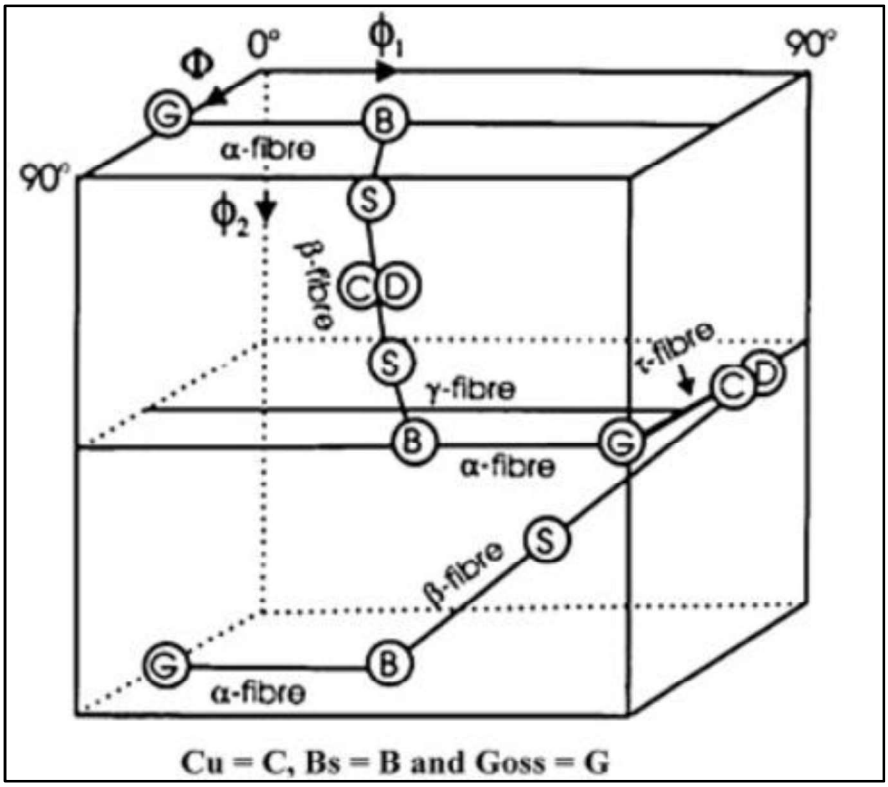

Fig. 1.15. Plots of important fiber textures in FCC-based metals, and alloys [111].

The α-fiber (Φ_2=0º section, Φ = 45º, and Φ_1= 0-35º) is the characteristic feature of the high stacking fault energy (high SFE) materials. Moreover, τ-fiber is the symbol of materials with intermediate stacking fault energy (SFE~ 40mJ/m^2) [113]. The β and γ fibers are the most important textures of the FCC-based metals/ alloys. The β fiber spreads from {112} <111> through {123} <634> to {110} <112> (Fig. 23) [113]. At lower strains, the intensity of the β fiber could be best described by the homogeneous orientation [115]. Moreover, at higher strains high SFE materials display peaks near the S {123} <634> texture, while low SFE materials display peaks near the Bs {110} <112> texture. Some of the important fiber textures developed in FCC-based metals and alloys are given in Table 1.13.

Table 1.14 Important fibers texture in FCC-based metals and alloys [115].

FCC Fibre textures		
A	<011>//ND	**From** 0°, 45°, 0° **to** 90°, 54.7°, 45°
Γ	<111>//ND	**From** 60°, 54.7°, 45° **to** 90°, 54.7°, 45°
T	<011>//TD	**From** 90°, 0°, 45° **to** 90°, 90°, 45°
B	B	**From** 90°, 35°, 45° **to** 35°, 45°, 90°

1.23 Micro textures in 7075 Al-alloys

Microtexture shows collective information of the two terms, the first one relates to the crystallographic parameters, and the second term pertains to the microstructural parameters [113]. The former pertains to the orientation of the individual grains. Moreover, the latter deals with the morphology, size distribution, and crystal orientation [111]. The grain size, shape, grain orientation spread (GOS), grain average misorientation (GAM), and kernel average misorientation (KAM), low and high-angle grain boundary fractions are some examples of the micro-textures. Microtexture characteristics influence stress-corrosion cracking (SCC) because the nature of the failure is crystallographic [110]. It was observed

that the low-angle grain boundary and special coincidence site lattice (CSL) boundaries are crack-resistant, while the high-angle boundaries are prone to cracking [118]. The GOS shows the deviation of each measurement point in the grain from the average orientation of the grain [100]. GAM illustrates average misorientation of point-to-point misorientation within the grains. In KAM, for a given point in grain, the average misorientation of that particular point with all its neighbors is calculated [100]. The geometrically necessary dislocation (GND), statically stored dislocation (SSD), Taylor factors, coincidence site lattice (CSL), and boundaries are part of the micro-texture textures [119].

The mechanical, physical, and chemical properties of polycrystalline materials are influenced by the crystallographic texture. Texture introduces anisotropy in the properties, which changes with the direction. Textures, also influence the elastic moduli, strength, ductility, fracture toughness, and fatigue. Therefore, texture study becomes important before applying the 7075 Al alloys in the structural engineering application [111].

1.24 Structural phase transformations in age-hardenable Al-alloys

Generally, two possible combinations of structural phase transformations occur in the age hardenable Al-alloys. The first one relates to the nucleation and growth type of structural phase transformations, and the second is attributed to the spinodal decomposition-assisted phase transformations [53]. The former displays sharp composition fluctuations with a limited period. On the other hand, the latter shows long-range composition fluctuations over a prolonged period [120]. Room temperature ageing promotes the decomposition of SSSS (α) by spinodal decomposition [121]. Whereas, elevated temperature aging (120ºC, for 24hrs) forms the metastable precipitates by the nucleation and growth-assisted structural phase transformations [121]. The alloy used in the current study does not give the room temp. ageing treatment therefore spinodal decomposition was not discussed in details in this

doctoral thesis. Details of the phase transformations by nucleation and growth assisted route is given in the Fig. 1.16.

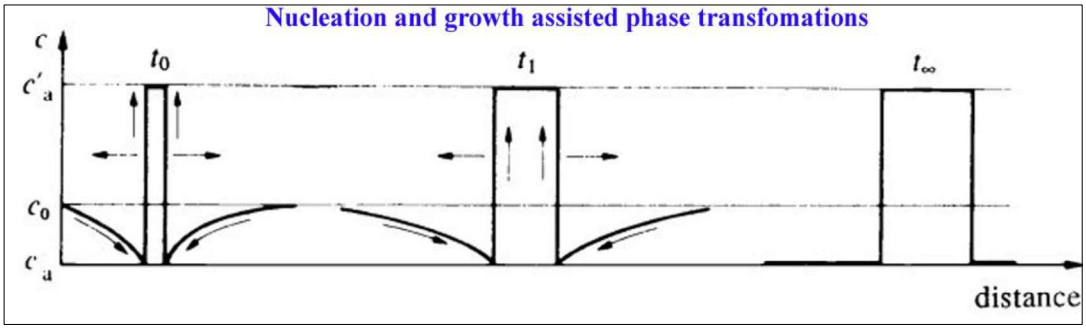

Fig. 1.16 Composition fluctuations during nucleation and growth-assisted structural phase transformations [76].

The coherent GP zone (aging below < 120 ºC) forms due to spinodal decomposition-assisted structural phase transformations [121]. Moreover, diffusion-assisted nucleation and growth are responsible for the formation of the η' and η precipitation [42,53].

During phase transformations, metastable phases minimize their free energy to maintain the ultimate equilibrium [25]. The alloys experience thermodynamic instabilities, if their excess free energy, $\Delta G = \Delta H - T\Delta S$, is positive. On the other hand, an equilibrium state is attained when free energy is negative ($\Delta G < 0$). Here, ΔG represents the excess free energy of materials, ΔH depicts the changes in the enthalpy, and ΔS, shows changes in the configurational entropy of the alloy system [21,54].

1.25 Types of interfaces in age hardenable Al-alloys

The nature of the interface significantly influences the properties of the alloy system. The metastable precipitates form two types of interfaces during their evolution. The first one relates to the homophase interface, whereas the second pertains to the heterophase interface. The grain, twin, tilt, twist, and coincidence site lattice (CSL) boundaries are a few examples of the first type of interface. Such interfaces are formed either in the α-matrix lattices or may evolve during the nucleation of the metastable precipitates. The internal interfaces could be best seen using the atomic scale structural investigations with the help of high-resolution HR-TEM imaging or HR imaging in STEM mode. Moreover, the heterophase interfaces are formed between the two distinct phases. For example, formations of the coherent (GP zone), semi-coherent (η'), and incoherent (η) precipitates in the age hardenable Al-alloys. In the coherent interfaces, two adjoining crystals maintain the lattice registry in age hardenable Al-alloys and their interfacial energy ranging from 0.01 to 0.05 J/m^2. The incoherent interface consists of the patches separated by the dislocation. Its energy is mainly elastic and the core energy of interfacial dislocation. The elastic energy of interfacial dislocation is taken to extend on either side up to half of the distance between neighbouring dislocations. The interfacial energy of the incoherent interface is 0.3 to 0.4 J/m^2, and there is a lattice mismatch between the parent and the product phase that differs by more than 25%. The interfacial energy of this interface is more than 1 J/m^2. The characteristic features of the coherent, semi-coherent, and in-coherent interfaces are shown in Figs. 1.17a-d.

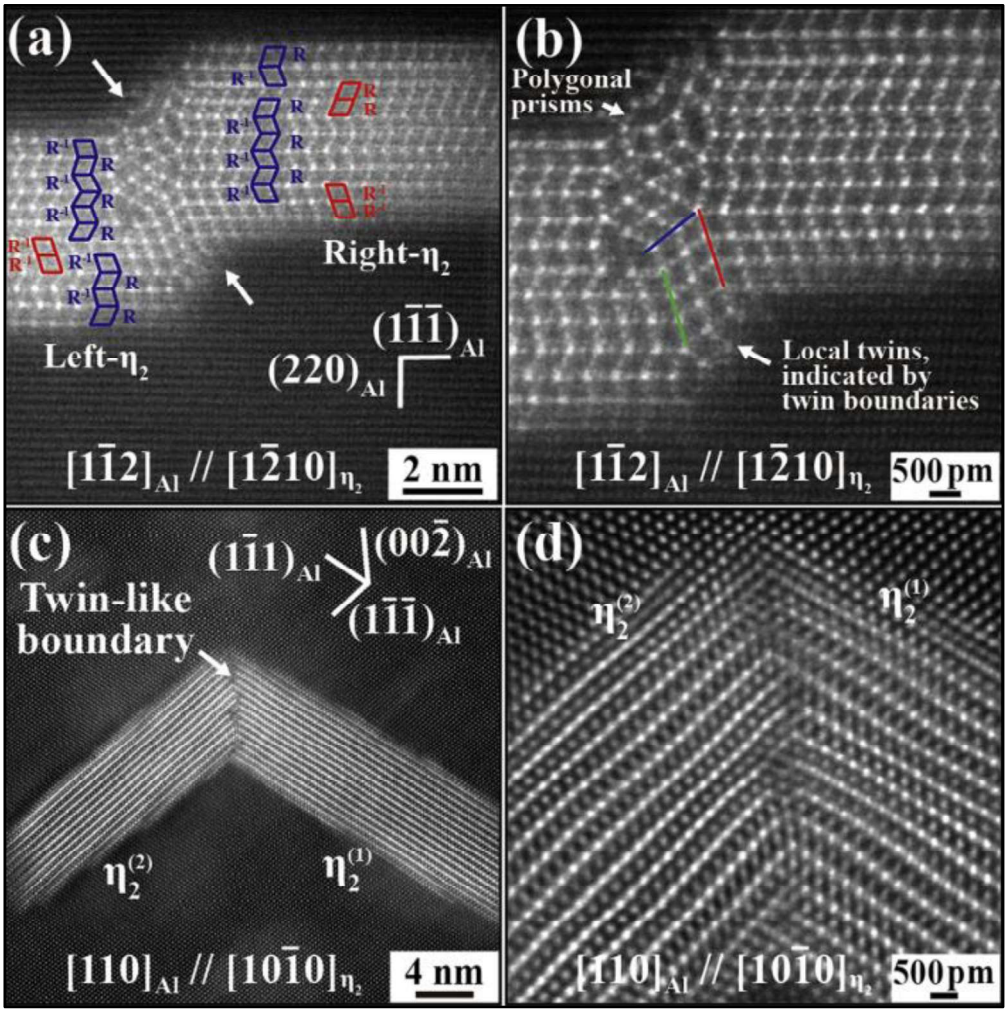

Figs. 1.17a-d Heterophase and homophase structure evolution in metastable precipitates, the interface between the matrix and precipitates show heterophase interface, and internal structures, like twin boundaries, and local twins created during nucleation and growth of precipitates display homophase interface [42,74].

1.26 Strengthening mechanisms

After showing the complete details of the age-hardening techniques. The strengthening factors, attributed to Al-Zn-Mg-Cu, 7xxx series Al -alloys are given below:

1.26.1 Grain size strengthening

The alloying additions, thermo-mechanical treatment, severe-plastic deformation (friction stir processing (FSP), equal channel angular pressing (ECAP), accumulative roll bonding

(ARB), multi-axial forging (MAF)), changes of the matrix grain size, and creates a high volumetric density of grain boundary which impedes the dislocation motion thus causes strengthening to alloy. Strengthening caused by grain boundary/ grain size is given by the Hall-Petch equation [122]:

$\sigma_y=\sigma_0+kd^{-1/2}$……*Eq. 1.3*

Here, d = average grain diameter, σ_0 = friction stress, k_y = Hall Petch constant.

1.26.2 Solid solution strengthening

Solid solution strengthening occurs if the other elements are alloyed with the metal matrix as solute atoms that differ from the matrix atoms in the size/ shear modulus, which may cause variation in the strain field. The local strain fields are created due to solute atoms that interact with the dislocation and cause hardening to the alloy systems, generally leading to improved yield strength. The widely accepted solid solution strengthening was given by the Fleischer equation, which is given below as [122,123]:

The solid solution strengthening, $\boldsymbol{\sigma_{ss} = MGb\varepsilon^{3/2}\sqrt{c}}$……..……...***Eq.1.4***

Here, M = mean orientation factor (3.06) for FCC polycrystalline materials, G = shear modulus, 26.9 GPa for α-Al, b = magnitude of the Burger vector, which is 2.86 Å for the α-Al. For the nanostructured grain materials (Grain size < 30 nm) the power of 'c' should be 1 instead of ½, and the value of $\Delta\sigma_{ss}$ strongly related to the differences in the shear moduli between the solute atoms and the α-Al [20]. The concentration "c" and the differences in the size between the solute atoms and the host atoms, cause the lattice-misfit or micro-strain (ε) in the α-Al matrix. The AA7075 alloy contains the Zn, Mg, and Cu solute atoms, and the differences in the atomic radius of the solute atoms contribute to the strengthening of the alloys. Differences in the atomic radius of the solute atoms contribute to increased yield-

strength of the alloys. Atomic radii of the major alloying elements used in the as-cast Al-alloys are given in Table 1.14.

Table 1.15 Atomic radii of alloying elements in 7xxx series Al-alloys [20,21]

S.N.	Alloying elements	Atomic radi (Å)	Differences in atomic radi (%)	Contribution on yield strength (MPa
01	Zn	1.38	-3.5	16
02	Mg	1.6	12	44
03	Cu	1.28	10.5	22
04	Fe	1.26	-12	
05	Cr	1.28	-10.5	
06	Si	1.11	-22.3	
07	Mn	1.79	25.17	
08	Zr	1.60	12	
09	Al	1.43		

1.26.3 Dislocation strengthening

Dislocation interacts with themselves and impedes their motion during the tensile plastic deformation, thus increasing the dislocation density and strength of the alloy. The significant strengthening caused by the dislocation in the 7xxx series of Al-alloys is given by the Bailey-Hirsch relationship [20]:

Bailey Hirsch relationship: $\Delta\sigma_d = M\alpha Gb\rho^{1/2}$..... *Eq.1.5*

1.26.4 Strengthening caused by metastable and equilibrium precipitates

Both the metastable precipitates (*GP zone, η', and η*) and dispersoids (Al_3Zr), as well as intermetallic compounds, e.g., Al2Cu(θ), Al2CuMg (S phase), cause strengthening in 7xxx series Al-alloy systems. Among them, strengthening caused by the precipitates and dispersoids is given by the Orowan dislocation bypassing/ shearing mechanisms [20]:

Orowan Mechanisms:

$$\Delta\sigma_{orowan} = M\frac{0.4Gb}{\pi\sqrt{1-\upsilon}}\frac{\ln(2\bar{r}/b)}{\lambda_p}$$ .....*Eq. 1.6*

Here, ν = poison's ratio of the α-Al, M, G, and b (in Å) were described in the previous sections

depending on the size and nature of precipitates. The shear stress required to force the precipitate particles from the dislocation is given by the following equation:

Shear stress, τ = Gb/l .....*Eq. 1.7*

Here, τ = shear stress required for dislocation motion, G = shear modulus (in GPa), b = magnitude of the burger vector (2.85Å for α-Al), and λ_p = length between two precipitates. The glissile dislocation faces two alternatives. Firstly, it can traverse the precipitate particles by either cutting through them. Secondly, it can bend around the precipitates and bypass them. Following the bypass, the dislocation forms loop structures around the precipitates. The cutting action occurs when the precipitates are either coherent with the matrix or possess an elastic modulus lower than that of the matrix and have a size smaller than 50Å.

If the precipitates are smaller than 50Å, the dislocation line "t" with the Burger vector "b" can cut through them. However, larger precipitates present a challenge during the interaction, requiring more shear stress (τ) to bypass them successfully. The reverse is also true in such precipitation scenarios. The resistance to dislocation motion increases in coherent precipitates due to the creation of steps after cutting through the precipitates. A higher volume fraction of precipitates makes moving the dislocation away from the precipitates more challenging. Precipitates with a higher elastic modulus demand tremendous shear stress to bypass them from the matrix than precipitates with a lower elastic modulus.

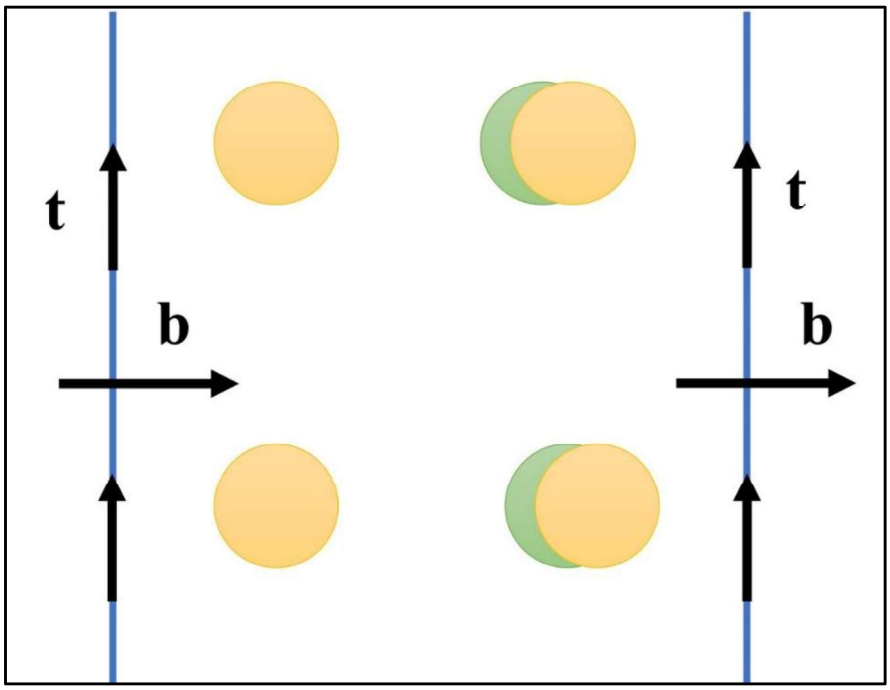

Fig. 1.18 Precipitates dislocation interaction, if precipitates are coherent and their size is less than 50Å [124,125].

If the size of the precipitates is large, ranging from 100Å to 500Å, and incoherent, they will bend around the precipitates and bypass them. Fig. 1.19 shows a schematic illustration of the interaction between a straight dislocation line 't' with a Burger vector 'b' and coherent precipitates in age hardenable Al-alloys. In Fig. 1.19a, the straight dislocation line 't' with a Burger vector 'b' is illustrated, separated by the distance 'L'. As shown in Fig. 1.19b, upon reaching equally spaced precipitates, the dislocation line with a distance 'L' bends around them. With further increasing stress, the dislocation line undergoes continuous bending until it reaches the critical radius, as shown in Fig. 1.19c. The stress required to bend the dislocation lines between two precipitates is given by *Eq. 1.5*. Upon reaching the critical radius (Fig. 1.19c), the dislocations begin to bulge out, and a segment of the dislocation meets, with opposite signs on each side of precipitates. Following the formation of loops around precipitates, the dislocation continues its movement, as shown in Fig. 1.19e.

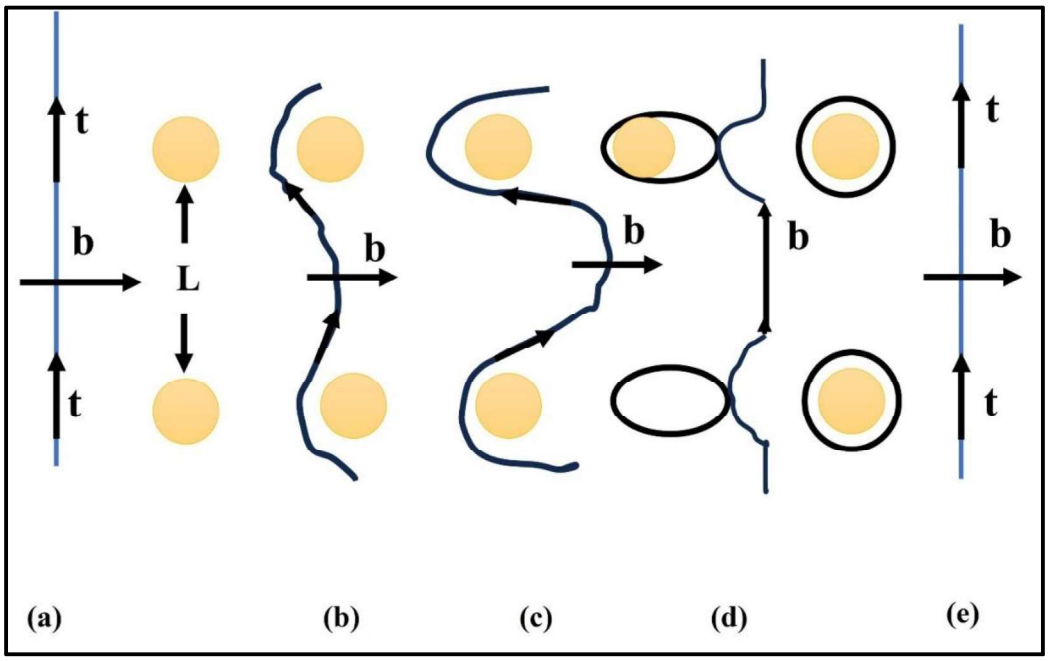

Figs. 1.19a-e Schematic display dislocation precipitate interaction if the precipitate particles are larger than 100Å to 500Å [124,125].

1.26.5 Constituents' particles

Dispersoids and other second-phase particle constituents are attributed to the intermetallic compound formed due to diffusion-assisted, structural phase transformation. These solutes are Si, Fe, Sn, and Mn, in addition to the few other alloying elements Ag, and Sc, in the α-Al (cF4). Such precipitates formed with Fe are insoluble in the α-Al. Moreover, the precipitates without Fe are entirely or partially soluble on account of the nature of the solute atoms. Larger constituent particles (> 1μm) are undesirable for the alloy matrix. However, such precipitates may enhance the crack growth and minimize the fatigue resistance and fracture toughness. Added to this, other strengthening factors, for instance, elastic modulus (E), disordering, stacking fault (SF), antiphase domain boundaries (APB), and interface between the matrix- precipitates also cause strengthening to the alloy. Yang et al. (2021) reported the significance of age-hardenable Al-Li alloys, as shown in Fig. 1.20.

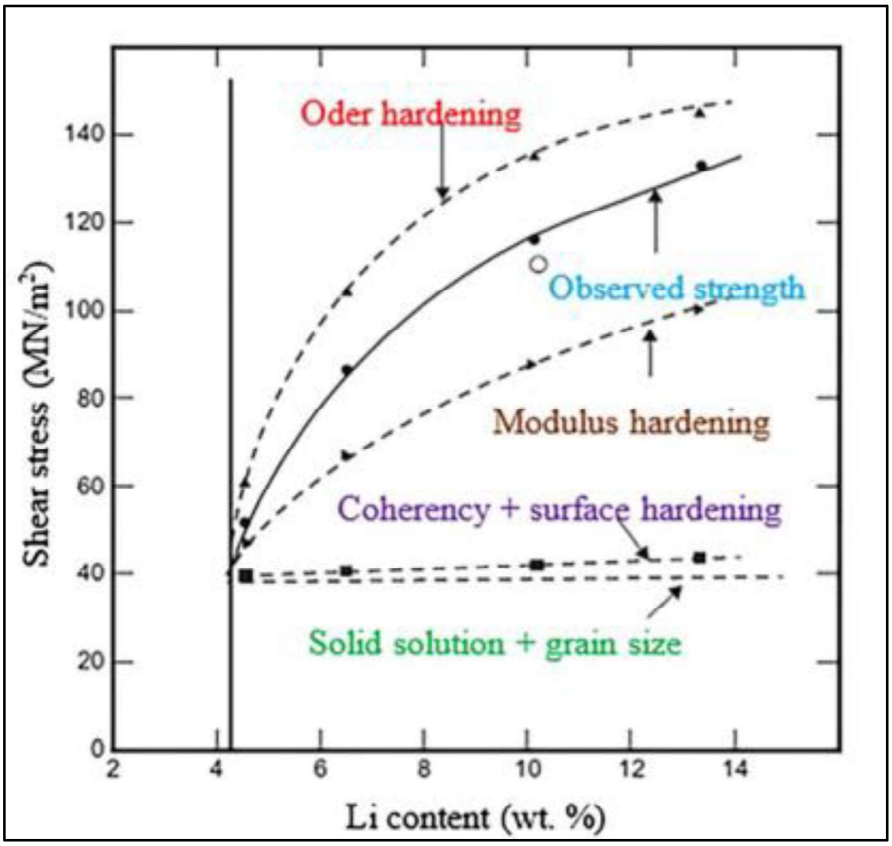

Fig. 1.20 Contribution of hardening factors in the Al-Li alloys [125A].

1.26.6 Aluminum alloy AA7075T7352

The alloy relates to the Al-Zn-Mg-Cu alloy system of the 7xxx series, which has been designed to obtain the high UTS to YS ratio and high work/ strain hardening exponent (n) so that it may deform uniformly without neck formation [90,126]. After solution treatment, the alloy was cold deformed to ~10% (at T7352 temper) to enhance the dislocation density in the α-Al matrix. After that, two steps of the ageing treatments, 120ºC for 24hrs, and over-ageing at a slightly higher temperature, 160 ºC, for 30hrs, were given. The deformation-assisted dislocation increases precipitation in the α-Al. Concurrently, these also form complex dislocation structures, thereby improving the mechanical properties by stopping the dislocation motion in the alloy matrix.

1.27 Methods for improving the performances of 7xxx series Al-alloys

The alloying additions [26,35], heat treatments [87,127,128], creep ageing [4], powder-metallurgy technique [129], thermo-mechanical treatment [30,31], and surface modification techniques (ultrasonic shot peening (USSP) [130], laser shock peening (LSP)[131], and friction stir processing [132]) are some of the methods used to improve the performance of alloys. Work carried out in this thesis includes heat treatments, cold rolling followed by ageing, and friction stir processing.

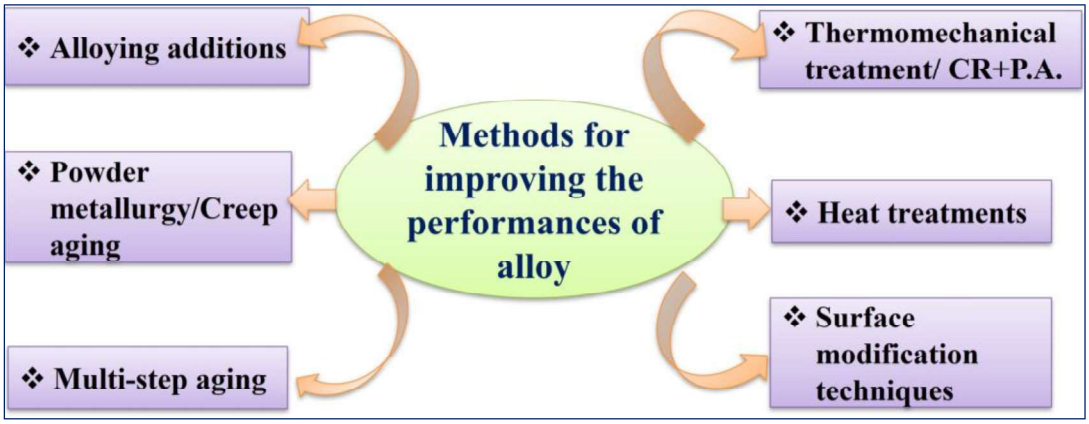

Fig. 1.21 Techniques used for improving the performances of 7075 Al-alloy.

1.28 Knowledge gaps

Based on the literature survey, specific knowledge gaps attributed to the above processing techniques were identified, and we have formulated particular objectives to address some of the issues associated with the above processing techniques in this doctoral thesis.

1.28.1 Knowledge gaps attributed to precipitation

On account of the literature survey, specific knowledge gaps pertain to the heat treated, cold rolled followed by peak ageing, and friction stir processing of the 7xxx series Al alloys and Al-Zn-Mg-Cu alloys were identified, and we have formulated particular objectives to address some of the issues associated with the techniques in this doctoral thesis.Precipitation behaviours of the 7xxx series Al alloys and Al-Zn-Mg-Cu alloy systems are well investigated, and different morphologies were reported. For instance, Zhao et al. (2004) reported spherical morphology of the GP zone in the ultrafine-grained 7075 Al alloy. Mukhopadhyay et al. (2009) reported plate morphology of the GP zone in a naturally aged Al-Zn-Mg-Cu-Zr alloy system. Variants of the GP zone, such as the GP-I and GP-II zone, were reported. GP-I is the solute-rich cluster, whereas the GP-II zone is represented as the vacancy-rich cluster.

The nucleation and growth behaviors of the η precipitates in the creep-aged 7050 Al-alloys were reported. However, nucleation and growth behaviors of the transition (GP zone, η') and equilibrium (η) precipitates, and the precipitation process of the AA7075T7352 were not extensively investigated. The DPs~ of the GP zone (I & II), and Al_3Zr dispersoids are confusing because the d-spacing value of Al_3Zr dispersoid (1.43 Å), and 220 of α-Al (1.43Å) are the same. Orientation relationships of the η' and η were reported in the case of the 7xxx series of Al-alloys and the Al-Zn-Mg-Cu alloys. However, orientation relationships of the GP zone, Al_3Zr dispersoid, and information of their DPs~ are lacking for the AA7075T7352.

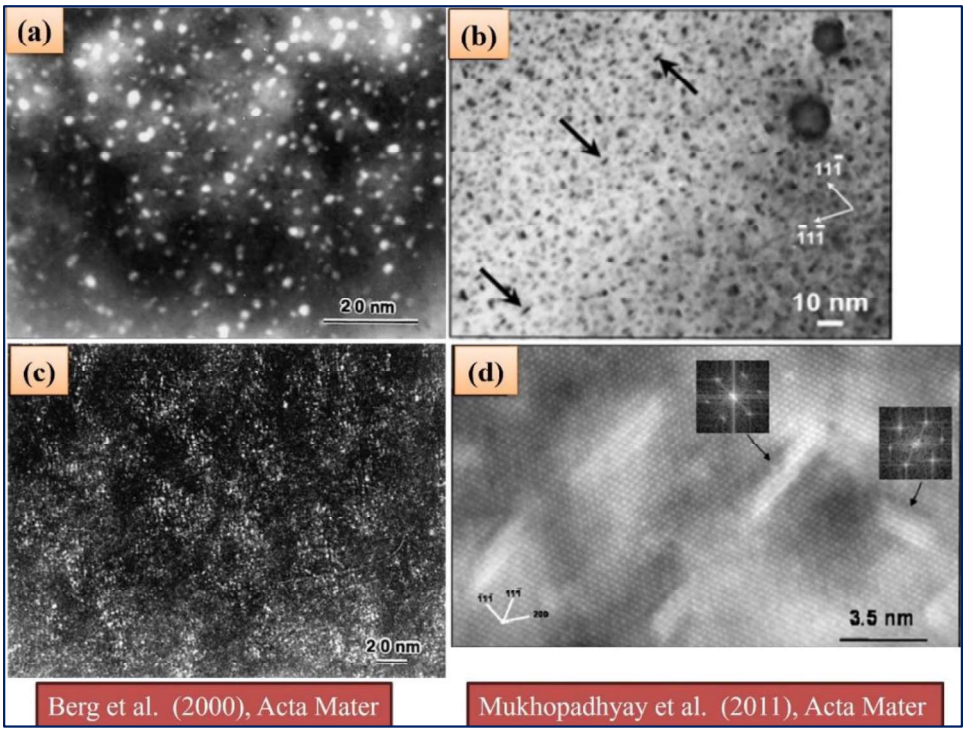

Figs. 1.22a-d Precipitates in 7xxx series of Al alloys: (a) solute rich clusters, (b) metastable precipitates (GP zone, η' and η), (c) vacancy rich clusters, (d) plate like morphology of the GP zone [48,133].

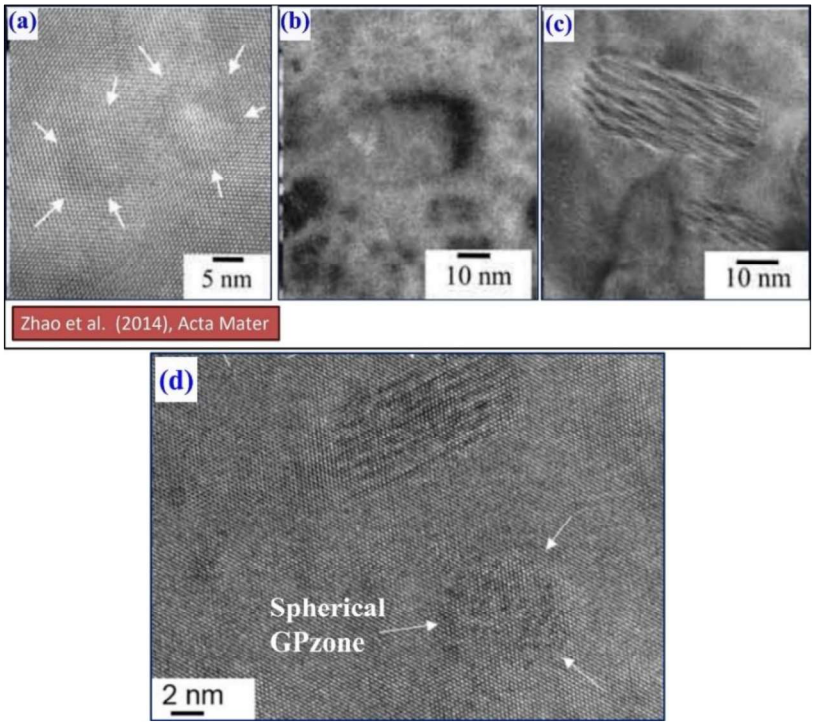

Figs. 1.23a-d Metastable precipitation in 7xxx series Al-alloy: (a) spherical precipitates, (b) rod like (η') phase, (c,d) plate-type η precipitates [43,122].

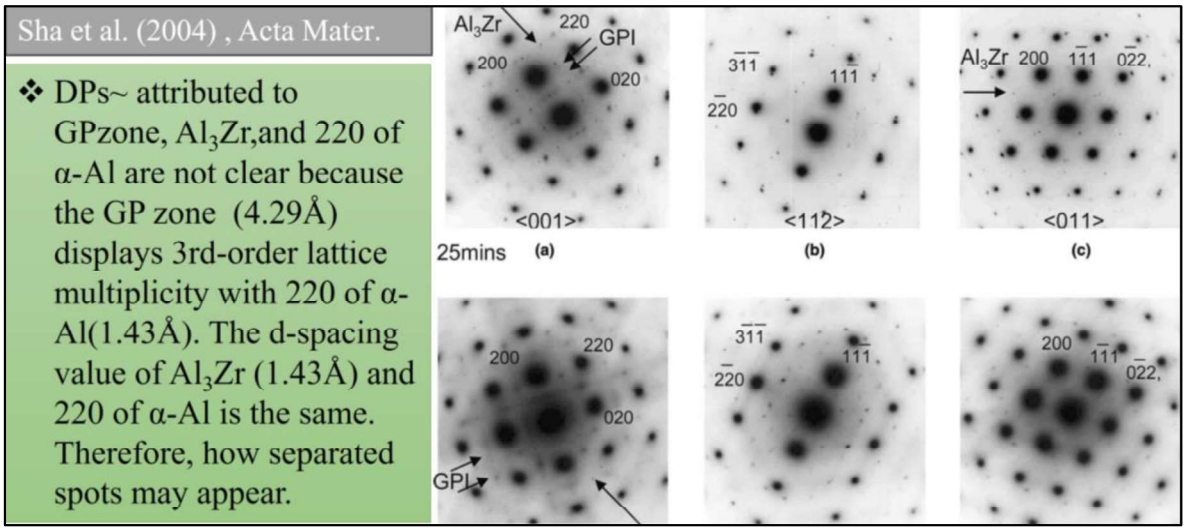

Fig. 1.24 Diffraction spots of 7075 Al-alloy showing GP I, and Al_3Zr dispersoids [46].

1.28.2 Knowledge gaps related to dislocation structures

The evolution of dislocation structures during plastic deformation is a critical factor in determining the suitability of materials for engineering airframe structures. This is because dislocation structures are strongly influenced by the strain field, a relationship extensively studied in the context of 7xxx series aluminum alloys, Al-Zn-Mg-Cu alloys, and the broader Al metallic system. However, there is a notable absence of investigation into the evolution of dislocation structures based on the strain field for AA7075T7352.

These alloys are specifically designed to achieve a high strain hardening exponent (n) and a high ultimate tensile strength (UTS) to yield strength (YS) ratio, both of which are directly linked to the evolution of the dislocation structures.

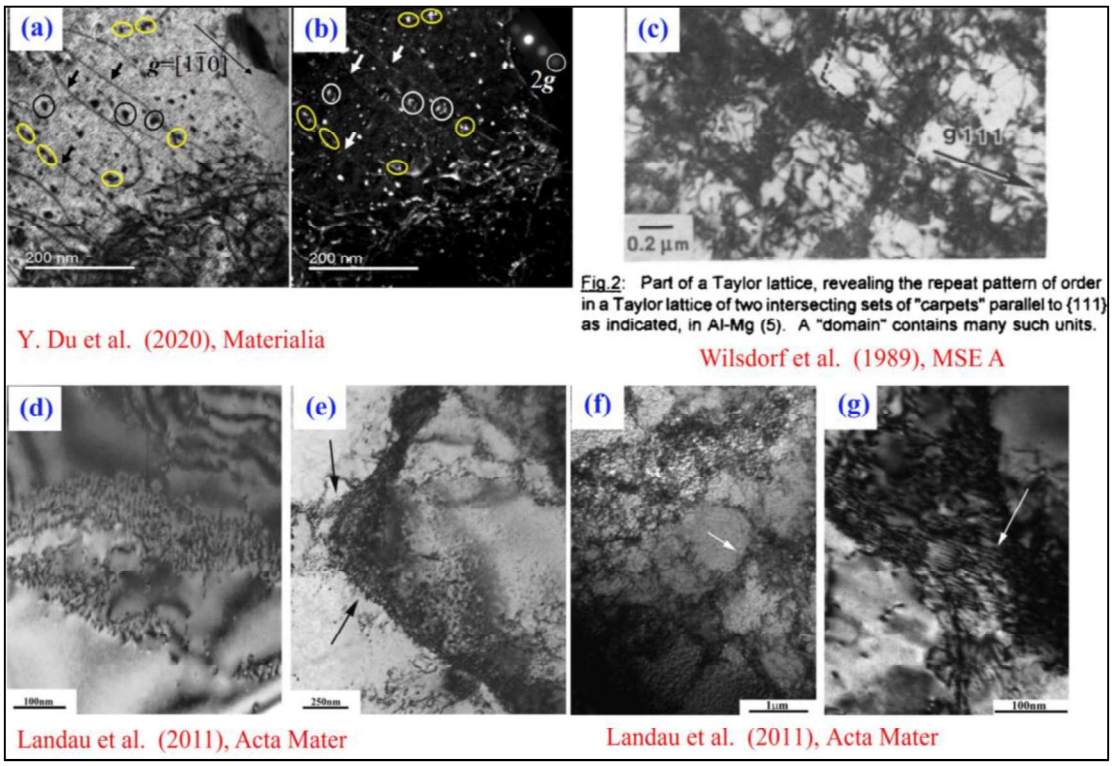

Figs. 1.25a-g dislocation structures in FCC cubic based metals and alloys: (a,b) dislocation loops, (c) Taylor lattices, (d,e) dislocation array, (f,g) cellular structures [95,96,134].

1.28.3 Knowledge gaps related to ageing and thermo-mechanical processing

Numerous scientific studies have addressed the precipitation behaviors and their impact on the strength, ductility, and stress corrosion cracking (SCC) performances, representing the 7xxx Al alloy, and Al-Zn-Mg-Cu alloys in the T4, T6, T73 tempered conditions [75,86,135,136]. However, the complex interplay among the relative precipitation behavior, texture characteristics, and residual stress in 7075 Al-alloys under T4, T6, T73, and T7352 tempers have not been elucidated so far. A comprehensive examination of flow behavior using well-established mathematical models such as Ludwik, Ludwigson, Hollomon, Voce, and Swift is notably absent. Furthermore, the correlation between flow curve parameters and precipitation behaviors, specifically concerning mechanical properties of AA7075 in T4, T6, and T73 tempers, has not been disclosed in the existing literature.

Despite the availability of substantial scientific investigations on Al-Zn-Mg-Cu and 7xxx series Al alloys, the diverse nature of alloys within the 7xxx series and Al-Zn-Mg-Cu alloys necessitates specific representation and investigations. While information regarding thermomechanical processing of 7xxx series Al-alloys has been reported, there is a notable gap in understanding the structure-property correlations resulting from a simplified thermo-mechanical treatment route, such as solution quenching (SQ) + cold rolling (CR) + peak-aging (PA) of 7075 aluminum alloys. The complex interplay among precipitation, dislocation structures, texture, and mechanical properties in this context has not been extensively explored.

1.28.4 Knowledge gaps related to friction stir processing

Friction stir processing (FSP) changes both the surface chemistry as well as microstructures in various processed zones. For instance, nugget zone (NZ), thermo-mechanically affected zone (TMAZ), heat-affected zone (HAZ), and base metal (BM), due to rotational motion of a tool in contact with the specimen surface [11, 34]. Additionally, the chemistry and microstructures also change along the longitudinal direction (top, middle, and bottom) due to temperature variations from top to bottom along the depth direction [14,22,137]. Notably, a paucity of literature addresses the evolution of microstructures and dislocation characteristics along the depth-wise direction. The friction stirring-assisted thermal effect and changes in the dislocation structures contribute to modification in the size and chemistry of fragmented precipitates [11, 34]. This phenomenon is exemplified by observations of two reverse trends involving dissolution and re-precipitation in the NZ of 7xxx series Al-alloys [39-42]. Studies by Liu et al. [138], and Su et al. [137] reported coarsening and evolution of new precipitates, while Sato et al. [139], Heinz et al. [104], and Jata et al. [140] reported dissolution of the phases. Consequently, these alterations in microstructures and chemistry

following FSP may impact the precipitation sequences, thereby influencing the mechanical, chemical, and physical performances of the alloy AA7075T7352, which is lacking in the literature. Surprisingly, the literature lacks discussion regarding microstructural evolution and its correlations with the mechanical properties resulting from the single and multi-pass FSP of AA7075T7352.

Given the widespread use of alloy AA7075T7352 in cyclic loading environments, crucial aspects such as low cycle fatigue, stress corrosion cracking behaviours, and the hardening exponent (n) remain unexplored in the existing literature. Addressing these gaps in knowledge is essential for a comprehensive understanding of the alloy's performance under various conditions.

1.29 Objectives

- To study in-depth microstructural and structural evolution of AA7075T7352, and tempered conditions of T4, T6, and T73.
- Investigation of the evolution of defect structures and its interaction with precipitates during partial straining of AA7075T7352 alloy.
- To study the evolution of microstructures and textures of thermo-mechanically processed 7075 Al-alloy.
- Correlations of microstructure and texture with mechanical properties of 7075 Al-alloy under different tempers and thermomechanical processing.
- To study the evolution of the microstructures, textures of friction stir processed AA7075T7352 and their effects on mechanical properties.